Astronomical calibration of the OAE1b from the Col de Pré-Guittard section (Aptian–Albian), Vocontian Basin, France

Fatima-Zahra Ait-Itto, Mathieu Martinez, Jean-François Deconinck, Stéphane Bodin

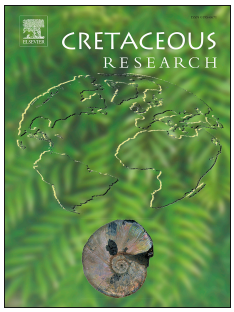

Astronomical calibration of the OAE1b from the Col de Pré-Guittard section (Aptian–Albian), Vocontian Basin, France

Fatima-Zahra Ait-Itto, Mathieu Martinez, Jean-François Deconinck, Stéphane Bodin

PII: S0195-6671(23)00146-5

DOI: https://doi.org/10.1016/j.cretres.2023.105618

Reference: YCRES 105618

To appear in: *Cretaceous Research*

Received Date: 16 December 2022

Revised Date: 25 May 2023

Accepted Date: 5 June 2023

Please cite this article as: Ait-Itto, F.-Z., Martinez, M., Deconinck, J.-F., Bodin, S., Astronomical calibration of the OAE1b from the Col de Pré-Guittard section (Aptian–Albian), Vocontian Basin, France, *Cretaceous Research*, https://doi.org/10.1016/j.cretres.2023.105618.

Ait-Itto Fatima-Zahra: I participated in the field trip, collecting and analyzing samples, and taking the lead in writing the original draft manuscript.

Mathieu Martinez: Significant contributions to the conceptualization and investigation of this work. which greatly contributed to the improvement of the manuscript. He's suggestions and inputs played a vital role in shaping the overall direction of the research.

Jean-François Deconinck : Participation in the field and sample collection with strong implication in the preparation and analysis of samples for $\delta^{13}C_{org}$ measurement was crucial to obtaining reliable data. Additionally, he made valuable contributions to manuscript correction and provided insightful recommendations, enhancing the quality of the final publication.

Stéphane Bodin: Contribution to the fieldwork, including sample collection and organic matter analysis (TOC/ HI/ OI) with significate contribution in the amelioration of the quality of the manuscript.

The collaborative efforts of all the co-authors were integral to the successful completion of this research. Their individual contributions, ranging from fieldwork to data analysis and manuscript improvement, have enriched the study's findings and its overall scientific value.

Astronomical calibration of the OAE1b from the Col de Pré-Guittard section (Aptian–Albian), Vocontian Basin, France

Fatima-Zahra Ait-Itto [a&b], Mathieu Martinez [a], Jean-François Deconinck [c], Stéphane Bodin [d]

a Univ Rennes, CNRS, Géosciences Rennes – UMR 6118, 35000 Rennes, France

b Univ Rennes, CNRS, Institut des Sciences Chimiques de Rennes, 35042 Rennes, France

c Biogéosciences, UMR 6282, CNRS, Université Bourgogne Franche-Comté, 6 Boulevard Gabriel, 21000, Dijon, France

d Department for Geoscience, Aarhus University, Hoegh-Guldbergs Gade 2, 8000 Aarhus C, Denmark

Abstract

A high-resolution spectral analysis was performed on magnetic susceptibility (MS) in the Col de Pré-Guittard section (CPG), Vocontian Basin, France to provide a new astronomical time scale of the Aptian-Albian transition and to explore the link between Milankovitch cycles and the occurrence of four laminated black shales events, namely Jacob, Kilian, Paquier and Leenhardt constituting the OAE 1b. The spectral analysis performed on the CPG section records the imprint of a strong predominance of the precession, and 100-kyr and 405-kyr eccentricity cycles. Based on the number of 405-kyr eccentricity cycles, the duration of the interval encompassing the Jacob to Leenhardt levels is calculated at 4.03 myr. The duration between Jacob, Kilian, Paquier and Leenhardt Events are respectively calculated at 1.55 myr, 1.62 myr, and 0.93 myr. The duration calculated for the occurrence of these events is not related to the Milankovitch cycles. However, these events are recorded near local maxima of the 405-kyr filter. Our results show that the 405-kyr eccentricity impacted the recurrence of anoxic levels in the Vocontian Basin, although additional factors, such as the emplacement of flood basalts or oceanic basaltic plateaus have contributed to the development of larger scale marine anoxia.

Keywords: Aptian – Albian, Cyclostratigraphy, Magnetic Susceptibility, OAE1b, Vocontian Basin

1. Introduction

The Aptian-Albian transition (~113 Ma) is punctuated by a series of widespread black shale deposits, collectively known as OAE1b. Four levels are frequently mentioned from the oldest to the youngest: Jacob, Kilian, Paquier, and Leenhardt levels (Bréhéret, 1985, 1988, 1997; Kennedy et al., 2000; Föllmi, 2012; Coccioni et al., 2014; Herrle et al., 2015; Matsumoto et al., 2020; Leandro et al., 2022). The Aptian-Albian boundary is located at the first occurrence of the planktonic foraminifer *Microhedbergella renilaevis*, within the Kilian Level (Kennedy et al., 2017) and the OAE 1b interval started at a time of decreasing temperatures, which reached a minimum near the Jacob or in between the Jacob and Kilian levels before increasing through the early Albian (McAnena et al., 2013; Bodin et al., 2015; Bottini et al., 2015; Bottini and Erba, 2018). This minimum in temperatures is described as the Aptian-Albian boundary cold snap (Mutterlose et al., 2009) and likely led to the development of polar ice (Price, 1999; Rodríguez-López et al., 2016). Within this broad trend, the anoxic levels corresponded to warm pulses (Wagner et al., 2008; Bottini and Erba, 2018), accompanied by rapid sea-level rise phases, increased weathering conditions, and detrital supply (Millán et al., 2014; Benamara et al., 2020) and decreased sea-surface salinity (Wagner et al., 2008). In pelagic environments, the anoxic layers marked a decrease in benthic foraminifera diversity and abundance, while opportunistic species prevailed (Erbacher et al., 1999; Friedrich, 2010). Species turnover and change in morphology occurred among the planktic foraminifera, likely in response to these paleoceanographic changes (Huber and Leckie, 2011). Radiolaria also experienced stepwise extinctions around the Aptian-Albian boundary (Erbacher and Thurow, 1997).

Questions arose on the forcing factor of these recurrent short-lived anoxic events. A negative Os-isotope excursion has been found in the Kilian Level in the Umbria-Marche Basin, that

correlate with the planktonic foraminiferal turnover suggesting a multiple submarine volcanic events (central Italy; Matsumoto et al., 2020). The link was confirmed by significant enrichments in Hg in DSDP Site 545, offshore Morocco, Eastern North Atlantic (Bracquart et al., 2022) suggest a link with the activity of the Kerguelen Plateau. Conversely, no evidence of volcanic activity has been found in the Paquier Level (Benamara et al., 2020; Matsumoto et al., 2020). According to the last Geologic Time Scale 2020, the duration between the OAE 1b events are; *ca.* 1.3 myr from the Jacob to the Kilian levels, *ca.* 1.9 myr from the Kilian to the Paquier levels and *ca.* 1 myr from the Paquier to the Leenhardt levels (Gale et al., 2020). These durations are close to the periods of the long obliquity cycle (1.2 myr) and long eccentricity cycle (2.4 myr) (Laskar et al., 2004), which questions the role of these long orbital cycles on the recurrence of anoxia around the Aptian-Albian transition (Wang et al., 2022). However, the durations estimated between the anoxic levels have demonstrated to be unstable from geologic time scale to another, which prevents from determining the forcing factors at the onset of these events.

Here, we perform spectral analyses on magnetic susceptibility signal acquired at very high-resolution in the Col de Pré-Guittard reference section (Albian GSSP, Vocontian Basin, SE France), in which these four well-exposed anoxic events have been defined (Bréhéret, 1997; Kennedy et al., 2017) to propose a new astronomical calibration of the Aptian-Albian transition and test the role of the orbital forcing on the inception of these anoxic events.

2. Geological setting

The Vocontian Basin (SE France) was located at a paleolatitude of 25-30 °N and corresponded to a paleo-passive margin between the NW part of the Alpine Tethys Ocean and the Atlantic Rift (Dercourt et al., 1993) surrounded by slopes and platforms (Fig. 1A, B). In the latest Hauterivian – early Aptian the basin was surrounded by the Urgonian carbonate platforms including the Provence platform to the South, the Ardèche-Vivarais platform to the West and Chartreuse-Vercors (Dauphiné platform) to the North. The Urgonian carbonate platform was drowned in the early Aptian and never recovered (Arnaud et al., 2017). After this event, during the Aptian-Albian, the Vocontian Basin was characterized by the deposition of the "Marnes Bleues" (Blue Marls) Formation, an hemipelagic marl-dominated sedimentation regime characterized by terrigenous fluxes comprising quartz and various clay minerals dominated by illite, smectite and kaolinite (Ghirardi et al., 2014, Corentin et al., 2020) mixed with biogenic components dominated by nannofossils and foraminifers. The paleo-water depth of the Vocontian Basin is estimated to have been several hundred meters based on palynological investigations (Wilpshaar and Leerveld, 1994). The Aptian-Albian transition is mainly composed by a monotonous succession of marly hemipelagic deposits intercalated by rare limestone layers and recurrent black shale levels (Bréhéret, 1997), some of these being prominent in the landscape in the Vocontian series and correlated at a supra regional scale (Jacob, Kilian, Paquier, Leenhardt). Slumps, turbidites and occasional diagenetic barite concretion accumulations are also observed (Bréhéret and Brumsack, 2000).

2.1 Studied section

The Col de Pré-Guittard outcrop is located in the northwestern part of the Vocontian Basin, SE France, near the village of Arnayon in the *Département de la Drôme* (F-26470), *ca.* 11 km northwest of Rémuzat and 2 km from la Motte-Chalançon (Fig. 2A). The section is well exposed over hundreds of meters. The lithological succession has been described in detail by Bréhéret (1997). It is characterized by monotonous sequences of marly hemipelagic to pelagic deposits of the Marnes Bleues Formation, in which intercalate limestone and black shale levels (Fig. 1C, D), among which are the Jacob, Kilian, Paquier and Leenhardt have been identified as prominent levels correlated beyond the Vocontian Basin. The Col de Pré-Guittard section is well studied, notably because it hosts the GSSP of the Aptian-Albian boundary (Kennedy et al., 2017). The Col de Pré-Guittard section has been chosen for our purpose considering both the detailed biostratigraphy and the lithology consisting mainly of monotonous hemipelagic marls with rare syn-sedimentary slumping, which are otherwise frequent in the Vocontian Basin (Friès and Parize 2003). The biostratigraphic divisions were established by ammonites (*Hypacanthoplites jacobi*, *Leymeriella germanica*, and *Leymeriella tardefurcata* Ammonite Zone), planktonic foraminifera, and calcareous nannofossils (Kennedy et al., 2000; Herrle et al., 2003). The studied section has been measured from the upper part of the Fromaget calcareous bundle (uppermost Aptian) to *ca.* 10 m above the Leenhardt horizon. It covers the four main black levels of the OAE 1b (Jacob, Kilian, Paquier, and Leenhardt).

2.2. Location of the GSSP section compared to Kennedy et al. (2017)

In the formal proposal of the GSSP of the Albian stage (Kennedy et al., 2017), the location of the GSSP section in their Figure 2 does not correspond to the picture shown in their Figure 3. After discussions, it appeared that it misled several teams working in the area, so we aim here at clarifying the location of the sections. The photograph picture of the section shown in Figure

3 of Kennedy et al. (2017) is actually located 1.38 km further NW (44°30′28″ N, 5°17′50″E). In our Figure 2A, it is labelled as "CPG-1 – GSSP". This section extends from the Jacob Event to the Kilian Event. In this section, the Kilian Level was labelled in the photograph picture in Kennedy et al. (2017) and perfectly observed as a prominent black shale layer. The Jacob Level corresponds to a black shale layer outcropping 1.5 m above a bundle of prominent limestone beds called "Fromaget bundle", also labelled in the photograph picture in Kennedy et al. (2017).

The section indicated as the GSSP in Figure 2 of Kennedy et al. (2017) is referred in our Figure 2B as "CPG-2" and extends from the Kilian Event to the Middle Albian. The Paquier Level is visible is the landscape as a prominent black shale horizon, as documented in the photograph picture in Figure 8 of Corentin et al. (2020). The Kilian and Leenhardt levels did not appear as prominent after a first investigation of the series, so we undertook 280 analyses of $\delta^{13}C_{org}$ measurements and 113 organic matter analyses to locate the Kilian and Leenhardt levels. Both the Kilian and the Leenhardt should appear with higher TOC and drastic increase Hydrogen Index (HI) in the organic-matter analysis. The Kilian Level should in addition be documented by a negative excursion both in $\delta^{13}C_{carb}$ and $\delta^{13}C_{org}$ (Herrle et al., 2004; Bodin et al., 2023). The samples were selected after performing the astrochronology of the section, so that there is at least a sample per precession cycle (~20 kyr). The intervals where we suspected the presence of the Kilian and the Leenhardt Levels were more densely covered. The intervals analyzed for spectral analyses are not affected by slumps. A decimetric glauconitic sandstone layer nonetheless outcrops at level 33.7 m in CPG-2. The durations calculated will be based on the longest cycles to limit the probability of missed cycles and the durations thereafter are described as minimum durations.

3. Material and methods

3.1. Field sampling

A total of 3249 samples were collected with a high-resolution stratigraphic step of 0.05 m recovering the four black levels (Jacob, Kilian, Paquier, and Leenhardt). The sample distance was selected to preserve the quality of the high frequencies. The measurements have been undertaken using a Jacob stick to limit the errors in the sample position. The weathered surface was removed and the samples were cleaned. The samples were crushed using a clean hammer and then weighted for magnetic susceptibility measurements. For chemical analysis, the samples were powdered using an agate mortar.

3.2. Magnetic susceptibility

The magnetic susceptibly (MS) measurement was conducted with Agico KLY-3 at the University of Rennes, in a total of 3249 samples were measured. The weighted samples are placed in a small plastic bag and introduced manually inside to the instrument. Before each series of measurements, an empty bag is measured for the blank correction and normalized to sample mass. The mass-specific MS is reported in m^3/kg.

3.3. Spectral analyses

Prior to the spectral analyses, the long-term evolutions of the magnetic susceptibility were calculated and subtracted using LOWESS method (LOcally WEighted Scatterplot Smoothing; Cleveland, 1979) to ensure the stationarity of the signal. Then, a multi-taper spectral analysis was performed using three 2π prolate tapers (2π-MTM spectrum; Thomson, 1982, 1990). The confidence levels against a red-noise were calculated using the robust procedure of Mann and Lees (1996). It consists in calculating the moving median over 20 % of the spectrum and fitting a red-noise model on this moving median. The confidence levels are then extrapolated assuming a χ^2 distribution. The spectral peaks exceeding the 95 % confidence levels are decreased to their

adjacent spectral power and the procedure is iterated another time. This procedure allows the spectral peaks not to be counted in the background estimation). Then a time-frequency weighted Fast Fourier transform (TF-WFFT; Martinez et al., 2015) was performed to trace the evolution of the periods along the sedimentary series. A correlation coefficient (COCO) was also applied to quantify which sedimentary rate leads to the best correlation between the spectrum of the sedimentary series and the spectrum of the orbital periods (Li et al., 2019). In this study 10.000 Monte Carlo simulations were applied to ensure stability of the results and reproducibility. Evolutive COCO (eCOCO) were also applied on each series. The size of the window was adapted to each series, depending on the estimated most likely sedimentation rates from COCO.

Each interpreted signal as orbital forcing is isolated and filtered using Taner lowpass and bandpass filters (Prokopenko et al., 2006). The sedimentary cycles were then anchored to their corresponding orbital periods, allowing depth-time conversions to be done. The orbital procedure used here assumes a constant duration of 405 kyr between two repetitions of the filter of the 405-kyr eccentricity cycle and a constant sedimentation rate between two consecutive anchor points. To precisely locate the black levels in the CPG-2, 290 samples were selected according to a precession 20-kyr filter to be analyzed on carbonate content, Total Organic Carbon (TOC), and carbon isotope on organic matter ($\delta^{13}C_{org}$).

3.4. Carbonate content and carbon isotope

The calcium carbonate content and $\delta^{13}C_{org}$ were measured on 280 powdered samples at Biogéosciences laboratory, Université de Bourgogne/Franche-Comté in Dijon, France. The $\delta^{13}C_{org}$ was measured on carbonate-free residues. Sample powders were reacted with HCl (2 N) at room temperature for 2 h to remove carbonate phases. Residues were rinsed with deionized distilled water until neutral, centrifuged (4500 rpm for 15 min), and dried at 50 °C overnight. Aliquots of dried decarbonated samples (~ 7–50 mg) were then weighed in tin capsules. The $\delta^{13}C_{org}$ measurements were performed on a Vario MICRO cube elemental analyzer (Elementar,

Hanau, Germany) coupled in continuous flow mode to an IsoPrime stable isotope ratio mass spectrometer (Isoprime, Manchester, UK). USGS40 L-Glutamic acid (C = 40.8 wt%; $\delta^{13}C_{VPDB}$ = -26.39 ± 0.04 ‰) and IAEA-600 Caffeine ($\delta^{13}C_{VPDB}$ = -27.77 ± 0.04 ‰) certified reference materials were used for calibration. The carbon isotopic composition is expressed in delta notation and reported in per mil (‰) relative to the Vienna Pee Dee Belemnite (V-PDB) standard; external reproducibility based on duplicate analyses of samples is better than ± 0.2 ‰ (1σ).

3.5. Total organic carbon (TOC)

The organic matter characterization was performed on samples from the CPG-2 section using the Hawk (Wildcat Technology) anhydrous pyrolysis carbon analysis system at the Lithospheric Organic Carbon (LOC) lab, Department of Geoscience, Aarhus University, Denmark. A total of 113 samples were measured and calibrated using IFP 160000 standard. Precision and accuracy of measurements were better than 5 %. Four parameters are considered here: total organic carbon (TOC, wt%), oxygen index (OI, mg CO2/g TOC), Hydrogen index ((HI, mg HC/ g TOC, HC = hydrocarbons), and Tmax(°C)**.**

4. Results

4.1. Magnetic susceptibility

In Col de Pre Guittard section 1 (CPG-1), the mass-specific magnetic susceptibility (MS) ranges from 3.05 $\times 10^{-8}$ m^3/kg to 6.66 $\times 10^{-8}$ m^3/kg (Fig. 3). The MS series has an average value of 5.27$\times 10^{-8}$ m^3/kg. The long-term trend of the MS signal (red curve) shows a low average value around 4.94$\times 10^{-8}$ m^3/kg in the first 23 m of the section, which corresponds to the most carbonated interval. Then, from level 23 m to 38 m, the trend shows a higher value reaching an average nearby to 5.65$\times 10^{-8}$ m^3/kg, which corresponds to an increase in detrital component (Fig. 3A). After the short period of decreasing average MS values, from level 38 m to 48 m, the

trend in the MS values increases again from the Kilian Level to the top of CPG-1 to reach 5.60×10^{-8} m^3/kg.

In Col de Pré-Guittard section 2 (CPG-2), the mass-specific MS series range from 7.57×10^{-9} m^3/kg to 6.44×10^{-8} m^3/kg with an average value of 4.34×10^{-8} m^3/kg. The long-term trend of the MS series (red curve) shows that the values decrease in the first 45 m. Then the values stabilized around level 45 m to the top of the section (Fig. 3B). In this interval, the $CaCO_3$ content has an average value of 47 % (measured on 290 samples). The MS and $CaCO_3$ are inversely correlated r = -0.63. Knowing that the Blue Marls are dominantly composed of clay minerals and $CaCO_3$, this suggests that the paramagnetic clay minerals (illite and smectite) control the SM signal (Fig. 4). This result was expected since previous works in the same formation highlighted this inverse correlation (Ghirardi et al., 2014).

4.2. Organic carbon isotope and pyrolysis analysis

The $\delta^{13}C_{org}$ values measured at CPG-2 range from -27.69 ‰ VPDB to -23.85 ‰ VPDB, with an average value of -25.88 ‰ VPDB (Fig. 3F). The $\delta^{13}C_{org}$ values show a broad increase from -26.5 ‰ VPDB at the base of CPG-2 to -25 ‰ VPDB at level 30 m. Then the values are stable at around -26 ‰ VPDB with higher-frequency fluctuations from level 30 m to the top of the section. The lowest $\delta^{13}C_{org}$ values drop to -27.69 ‰ and are observed at the base of CPG-2, together with HI values higher than 180 mgHC/gTOC) and TOC values higher than 2 % (Fig. 5A, B and C). These features perfectly align with the organic geochemical signature of the Kilian Level at Les Briers section (Fig. 5D, E and F), eastern Vocontian Basin (Bodin et al. 2023). According to these, the identification of Kilian level can be confidently proposed at the base of the section CPG-2.

The Kilian Level thus records the most negative value of the section with values around -27.69 ‰ followed by increasing values reaching -23.85 ‰ at 5 m. At 8.4 m, a prominent negative

235 excursion is recorded with values decreasing to -27.42 ‰, likely corresponding to the Horizon
236 Noir (HN1; Bréhéret, 1997), one of the dark horizons identified in the Vocontian Basin. In the
237 Paquier Level, the $\delta^{13}C_{org}$ registered a value around -26 ‰ at 53 m. Then, in the upper part of
238 the section, a distinct negative value of -27.08 ‰ VPDB is recorded, corresponding to the
239 Leenhardt Level. The Total Organic Carbon (TOC) contents at CPG-2 range from 0.53 wt% to
240 2.66 wt% (Fig. 3C) with an average value of 0.76 wt%. The long-term trend shows in general
241 values lower than 1 % with a significant increase in the values corresponding to the black level
242 reaching a maximum of 2.66 wt% in the Kilian Level. Furthermore, the Paquier and Leenhardt
243 levels record a small increase in TOC values reaching around 1.15 wt%. for both levels. The
244 Highest Hydrogen Index (HI) values are registered respectively at the Kilian (188
245 mgHC/gTOC), Paquier, (88 mgHC/gTOC) and Leenhardt (163 mgHC/gTOC) (Fig. 3D). The
246 rest of the samples register values less than 50 mgHC/gTOC. The Oxygen Index (OI) values
247 range from 20 to 114 $mgCO_2$/gTOC with an average of 40.50 $mgCO_2$/gTOC; (Fig. 3E).
248 Significant increase on TOC and HI below the Paquier Level, at 49 m, corresponds to HN8
249 (Bréhéret, 1997).

250 **4.3 Spectral analyses**

251 **4.3.1 CPG-1**

252 The spectral analysis performed on the MS series in Col de Pré-Guittard section (CPG-1) shows
253 the presence of significant periods with confidence level higher than 99 % at 10 m, 3.6 m, 1.8
254 m, 1.5 m, 0.66 m, 0.54 m and 0.48 m (Fig. 6A). A spectrogram was performed on 25-m width
255 windows focusing on the lowest frequencies (Fig. 7C). Another spectrogram was performed on
256 10-m width windows after filtering the lowest frequencies with a Taner low-pass filter in order
257 to focus on the high frequencies (frequency cut: 0.2171 cycles/m, Fig. 7D). CPG-1 first interval,
258 from levels 0 m to 25 m, shows the predominance of two bands at 12 m and 0.65 m (Figs. 7C,
259 7D). Another band is observed with high amplitudes from 10 to ~30 m at 3.4 m (Figs. 7C, 7D).

A last band is observed with lower amplitudes around 1.5 m at level 6 m. The second interval, from level 25 m to the top of CPG-1, shows the presence of a band at 8.6 to 8.7 m with low amplitudes up to 43 m and then with high amplitudes (Fig. 7C). Two other group of periods are recorded from 1.6 to 2.7 m and from 0.47 m to 0.45 m (Fig. 7D). Two periods at 0.95 and 0.71 m appear punctually, respectively at level 30 m and at the top of the series.

The COCO method applied to the CPG-1 show the highest significant correlation at (*p*-value $<1\times10^{-3}$) at sedimentation rates around 0.8 cm/kyr, 1.7 cm/kyr, 2.7 cm/kyr, and 3.5 cm/kyr (Fig. 6B). The eCOCO procedure applied on 25-m width windows show a significant correlation at sedimentation rates around 3.5 cm/kyr and 2.5 cm/kyr from level 0 m to level 25 m then the sedimentation rate decreases to reach 1.9 cm/kyr from level 25 m to the top of the section. (Fig. 7E). According to the spectral analysis, the section can be subdivided in two intervals to limit the effect of the sedimentation: Interval 1 from level 0 m to 30 m, in which the sedimentation rate is around 3 cm/kyr, and interval 2 from 25 m to the top of the section, in which the sedimentation rate is around 2 cm/kyr. We left 5 m of recovery between intervals 1 and 2 to ensure continuity of the filters (Fig. 7B).

The 2π-MTM spectrum performed on Interval 1 of CPG-1 (from level 0 m to 30 m) shows the presence of significant spectral peaks at 14 m, 3.4 m, and from 0.72 m to 0.43 m exceeding the 99 % confidence level (Fig. 6C). The COCO analysis recorded shows a highly significant correlation (p-value <1×10-3) at sedimentation rates at 3.5 cm/kyr additional correlation is registered around 2.7 cm/kyr (Fig. 6D). The 2π-MTM spectrum performed on Interval 2 of CPG-1, from level 25 m to the top of the section, shows the presence of a significant peak at the 2π-MTM spectrum with a confidence level higher than 99% at 8.7 m, 2.4 m, 1.6 m, 0.46 m and 0.34 m (Fig. 6E). An additional period is recorded with a confidence level exceeding 95% at 0.56 m. The COCO method applied to Interval 2 of CPG-1 shows a highly significant correlation at a sedimentation rate of 1.9 cm/kyr. Additional significant correlations are

observed around 2.2 cm/kyr, 2.5 cm/kyr and 1.3 cm/kyr with however less confidence (Fig. 6F).

4.3.2 CPG-2

The 2π-MTM spectrum performed along CPG-2 shows the presence of significant periods with a confidence level higher than 99% at 20 m, 10 m, 6.9 m, 3.6 m, 1.5 m, 1.0 m and 0.74 m. In addition, periods at 2.2 m and 1.2 m exceed the 95 % confidence level (Fig. 8A). A spectrogram was performed on 40-m width windows to focus on the lowest frequencies (Fig. 9C). Another spectrogram was performed on 15-m width windows after filtering the lowest frequencies with a Taner low-pass filter in order to focus on the high frequencies (frequency cut: 0.1319243cycles/m, Fig. 9D). The spectrogram focused on the low frequencies shows a low-amplitude band with periods of 15 and 8 m from the base of the series to level 25 m (Fig. 9C). These low frequencies show then a bifurcation to high-amplitude period of 30 m and a lower-amplitude period of 10 m. This bifurcation is observed from level 25 m to 70 m (Fig. 9C). This band then stabilizes to periods ranging from 26 m to 20 m from level 70 m to the top of the series (Fig. 9C). An additional band is recorded with periods increasing from 3.2 m to 4.2 m, from the base of the series to level 35 m. Periods of 6.8 to 3.6 m are observed from level 35 m to 80 m (Fig. 9C) and periods of 5.1 to 3.3 m are observed from level 85 m to the top of CPG-2 (Fig. 9C). At higher frequencies, periods around 1.5 m 0.74 m are recorded throughout CPG-2 with low amplitudes (Fig. 9D).

The COCO analysis along the CPG-2 shows highest correlations at (p-value $<1\times10^{-3}$) at sedimentation rates of 2.5 cm/kyr, 3.3 cm/kyr, 5.3 cm/kyr and 7 cm/kyr (Fig.8B). The eCOCO analysis performed on 40-m width windows shows significant correlations between the spectra of the sedimentary and astronomical series at the sedimentation rate around 2.4 cm/kyr, 3.3 cm/kyr from levels 0 m to 30 m (Fig. 9E). From level 30 m to the top of the section, most

309 significant correlation is observed at sedimentation rates decreasing from 7.2 cm/kyr at level
310 27 m to 4 cm/kyr at the top of CPG-2.

311 Based on the evolutive spectral and eCOCO analyses, CPG-2 was divided into an interval from
312 0 to 30 m, in which the most likely sedimentation rate appears to be around 3 cm/kyr, and from
313 20 m to the top of CPG-2, in which the most likely sedimentation rate is higher and
314 progressively decreases throughout the interval (Fig. 9E). The 2π-MTM spectrum performed
315 on Interval 1 of CPG-2 (from 0 m to 30 m), show significant periods with confidence levels
316 higher than 99% observed at 7.5 m, 2.1 m, 1.0 m and 0.73 m (Fig. 8C). Two periods exceeding
317 the 95 % confidence level are observed at 1.6 m and 0.33 m, and two periods exceeding the 90
318 % confidence level are observed at 0.47 m and 0.37 m. The COCO analysis performed on
319 Interval 1 of CPG-2, indicates that the highest significant correlations (p-value $<1\times10^{-3}$) is at a
320 sedimentation rate of 2.5 cm/kyr (Fig. 8D). In Interval 2 of CPG- 2 (from 20 m to the top), the
321 2π-MTM spectrum shows spectral peaks at 22 m, 7.3 m, 3.7 m, 1.5 m, 0.94 m, 0.83 m and 0.75
322 m exceeding the 99 % confidence level (Fig. 8E). The COCO analysis shows a high significant
323 correlation (p-value <1×10-3) at sedimentation rates at 5.5 cm/kyr, and 7.1 cm/kyr (Fig. 8F).

324 **5. Discussion**

325 **5.1. Interpretation of the sedimentary cycles for CPG-1**

326 The signal processing along the CPG-1 indicates two intervals with an average sedimentation
327 rate of 3 cm/kyr from 0 to 30 m and of 2 cm/kyr from 30 m to the top of the series (Fig. 7E). In
328 previous spectral analyses, an average sedimentation rate of 3 cm/kyr was estimated for the
329 upper Aptian in hemipelagic deposits of the Vocontian Basin, SE France (Heimhofer et al.,
330 2004; Kößler et al., 2001). The present analysis confirms and refines these previous estimates.
331 From COCO, eCOCO and spectral analyses, the thickness of the 405-kyr eccentricity cycle
332 evolves from an average of 14 m in Interval 1 of CPG-1 to 8.7 m in Interval 2 of CPG-1. The

thickness of the 100-kyr eccentricity cycle evolves from 3.4 m in Interval 1 to ~2 m in Interval 2 (with a range from 2.7 to 1.6 m). The thickness of the precession cycles evolves from 0.65 m in Interval 1 to 0.46 m in Interval 2 (Fig. 7). The 405-kyr eccentricity cycle was extracted using a Taner lowpass filter performed on the whole of CPG-1 with a higher frequency cut of 0.1648 cycles/m (Fig. 7B). In addition, the 100-kyr eccentricity band was extracted using Taner bandpass filters with lower and higher frequency cuts of 0.1833 and 0.6000 cycles/m in Interval 1, and lower and higher frequency cuts of 0.2365 and 0.7095 cycles/m in Interval 2. The filter of the 405-kyr eccentricity cycles shows 4 repetitions at CPG-1, implying a total duration of the sampled interval of 2.38 myr and duration of the interval from the base of the Jacob to the base of the Kilian event of 1.55 myr.

A recent dataset published by Charbonnier et al. (2023) estimates from an eCOCO analysis a sedimentation rate of 4.5 cm/kyr in CPG-1, which leads to a duration of 0.8 myr between the Jacob and Kilian events. Charbonnier et al. (2023) used a window size of 60 m to perform the eCOCO analysis. The most likely sedimentation rate calculated from this approach is 5.8 cm/kyr, decreasing to 4.3 cm/kyr in the topmost 60 m of the series (Fig. 10D). However, a TF-WFFT applied on the series with 15-m width windows shows that the periods of the highest frequencies evolve from 1.3 to 1.6 m from the bottom of L5 to 300 m, and then decrease down to 0.3-0.4 m in the topmost 20 m of the series (Fig. 10C, see also Fig. S1D in the electronic supplement). Another eCOCO analysis applied on 25-m width windows (Fig. 10E) shows most likely sedimentation of 4.0 to 6.0 cm/kyr from 300 to 320 m, 3.4 cm/kyr 330 to 375 m and 2.2 cm/kyr in the topmost part of the series. We performed three 2π-MTM analyses from the base of the series to 320 m (Interval 1), from 315 m to 365 m (Interval 2) and from 360 m to the top of the series (Interval 3; Figs. 10F-H).

The 2π-MTM spectrum of Interval 1 shows periods at 22 m, attributed to the 405-kyr eccentricity cycle, from 6.7 m to 4.0 m, attributed to the 100-kyr eccentricity cycle, from 2.5 to

1.9 m, attributed to the obliquity, and from 1.6 m to 0.85 m, attributed to the precession (Fig. 10F). The 2π-MTM spectrum of Interval 2 shows periods at 17 m, attributed to the 405-kyr eccentricity cycle, from 3.8 m to 2.2 m, attributed to the 100-kyr eccentricity cycle, from 1.7 to 1.0 m, attributed to the obliquity, and from 0.7 m to 0.50 m, attributed to the precession (Fig. 10G). The 2π-MTM spectrum of Interval 3 shows periods at 8.6 m, attributed to the 405-kyr eccentricity cycle, from 2.2 m to 1.5 m, attributed to the 100-kyr eccentricity cycle, and from 0.55 m to 0.29 m, attributed to the precession (Fig. 10H). These spectra performed on these intervals agree with the broad variations in the sedimentation rates calculated from eCOCO with window sizes of 25 m.

This comparison highlights that eCOCO analyses, as well as evolutive FFTs, are sensitive to the sizes of the windows chosen. Long window sizes are efficient to calculate large sedimentation rates. However, they cannot capture their rapid variations within the sedimentary series. Conversely, short window sizes can be efficient to capture these rapid variations in the sedimentation rates. Thus, by focusing on Col de Pré-Guittard series, our study is able to observe this decrease in the sedimentation in the last 20 m of CPG-1.

5.2. Interpretation of the sedimentary cycles for CPG-2

The signal processing along the CPG-2 indicates an average sedimentation rate of 3 cm/kyr from 0 to 30 m and a sedimentation rate varying from 4 cm/kyr to 7 cm/kyr in the remaining part of the series (Fig. 9E). From COCO, eCOCO and spectral analyses, the thickness of the 405-kyr eccentricity cycle evolves from an average of 13 m from level 0 to level 43 m, an average of 11 m from level 43 m to level 54 m, and an average thickness of 23 m in the remaining part of the studied series (Fig. 9B). The 100-kyr eccentricity cycle has a thickness ranging from 3 to 4 m from the base of the series to level 32 m, and thicknesses ranging from 7 m to 3 m from level 32 m to level. The obliquity is well expressed from the base of the series to level 32 m. Then the precession has higher amplitude with thicknesses ranging from 1.5 m

to 0.7 m to the top of the series. Our calibration shows that 405-kyr eccentricity cycles Ab405-3 and Ab405-4 contain six repetitions of the 100-kyr eccentricity altogether. This interval contains the glauconitic sandstone layer associated to a short-term hiatus which duration could be assessed at 200 kyr provided that no complete 405-kyr eccentricity has been erased.

The 405-kyr eccentricity cycle was extracted using a Taner lowpass filter with a higher frequency cut of 0.1648 cycles/m. The 100-kyr eccentricity cycle was extracted using a Taner bandpass filter with a lower and higher frequency cut of 0.2167 cycles/m and 0.5667 cycles/m in Interval 1 and lower and higher frequency cuts of 0.1251 cycles/m and 0.3527 cycles/m in Interval 2. The filter of the 405-kyr eccentricity cycles shows 6 repetitions at CPG-2 and implies a minimum duration of deposit of 2.63 myr. This duration is qualified as "minimum" to account for the potential hiatus linked to the glauconitic sandstone layer. The minimum duration between the base of the Kilian and the base of the Paquier levels is assessed at 1.62 myr and the duration between the Paquier and the Leenhardt levels is assessed at 0.93 myr.

Recent $CaCO_3$ data have been published from the Les Briers section, in the eastern part of the Vocontian Basin from the Kilian to Paquier levels (Bodin et al., 2023). The data have been measured with a median sample distance of 1 m. Assuming an average sedimentation rate of 3.8 cm/kyr between the Kilian and Paquier events at Les Briers (60 m between these events, duration: 1.6 myr), this represents a time of 26 kyr, enough to detect the 405-kyr eccentricity cycle at least. The $CaCO_3$ signal is selected for performing spectral analyses in Les Briers as it is inversely correlated to the MS signal in the Marnes Bleues Formation (see Fig. 4 and Ghirardi et al., 2014).

The $CaCO_3$ signal was linearly interpolated every 50 cm and detrended applying a LOWESS with a coefficient of 0.3 (Fig. 11C). The 2π-MTM spectrum of the detrended $CaCO_3$ signal shows spectral peaks at 17 m, exceeding the 99 % CL (Fig. 12), which represents a duration of 0.4 myr, assuming a sedimentation rate of 3.8 cm/kyr. The 17-m peak could thus represent the

405-kyr eccentricity cycle. The Taner lowpass filter of the peak at 17 m shows 4 repetitions between the Kilian and the Paquier, in agreement with the finding at CPG-2(Fig. 11D). This suggests that the hiatus associated with the calciturbidite event did not erase a complete 405-kyr eccentricity cycle and thus did not affect the duration estimates between the Kilian and Paquier events.

5.3 Forcing factors of Aptian–Albian black shales

Our astrochronology based on 405-kyr filter recorded at CPG-1 and CPG-2 shows that eleven repetitions of the 405-kyr eccentricity cycles are recorded in the studied interval. The Jacob Level is located at the boundary between E405-1 and E405-2 (Fig. 7), while the Leenhardt Level is located less than 0.1 myr below the top of cycle Ab405-6 (Fig. 9), leading to a duration from the base of the Jacob Event to the top of the Leenhardt Event, so-called OAE1b interval, of 4.03 myr. Interestingly, the duration of the OAE1b interval calculated here is in close agreement to the duration of 4.27 myr proposed for the OAE 1b interval in the Geologic Time Scale 2020 (Gale et al., 2020), suggesting again that the hiatus related to the glauconitic sandstone did not erase a complete 405-kyr eccentricity cycle. The duration between the four events (Jacob, Kilian, Paquier and Leenhardt) are respectively 1.55 myr, 1.62 myr and 0.93 myr. These durations do not follow the long eccentricity and obliquity cycles (2.4 myr, and 1.2 myr, respectively). This suggests that the long orbital cycles are not responsible for the inception of the main anoxic events of the OAE 1b interval. However, these four events all locate just below a maximum in the filter of the 405-kyr eccentricity cycle, suggesting that this eccentricity could have impacted, in addition to another forcing factor, the onset of the events.

Caillaud et al. (2022) attribute the concomitant accumulation of organic matter during the oceanic anoxic events (OAE 1b) to various parameters such as productivity, sea level, sedimentation, and accumulation rates with the influence of regional factors. In Poggio le

Guaine (Umbria-Marche Basin, central Italy), two negative spikes in Os isotopes below the Kilian level, together with mercury enrichments in the OAE 1b interval, suggest a link between this event and the multi-phase emplacement of the southern Kerguelen plateau in the late Aptian-early Albian (Matsumoto et al., 2020; Sabatino et al., 2018). The emplacement of the southern Kerguelen plateau (Indian Ocean) coincides with the Aptian-Albian transition (113 Ma) and correspond to the production of 2.5 x 10^7 km^3 of mafic crust (Coffin et al., 2002). Conversely, Benamara et al. (2020) show a lack of significant Hg enrichment in the Paquier Level suggesting that this event is not linked to Kerguelen plateau LIP activity. Finally, Bracquart et al. (2022) noted that in DSDP Site 545 off Morocco, mercury enrichment occurred *ca.* 5-6 m below the Kilian Event, corresponding to *ca.* 200-250 kyr, assuming a thickness of 40 m between the Kilian and Jacob events and our time scale (Herrle et al., 2004). These two last studies show that the volcanism is not the sole forcing factor to the onset of these anoxic episodes. Hence, Wang et al. (2022) showed that pronounced global deoxygenation period occurred only during the Paquier event, which was related to warmer climate and increased nutrient levels linked to the long-term influence of the Kilian event triggering volcanism modulated by orbital parameters. In a context of a series of volcanic pulses linked for instance to the emplacement of the Kerguelen Plateau, the modification of the seasonality may act as an additional forcing factor which contributed the climate system to pass a threshold leading to widespread anoxia. Jovane et al. (2006) and Leandro et al. (2022) presumed that the continental runoff occurred during wetter climate phases which occurred during the seasonal variability during eccentricity maxima.

5.4. Implications for the timescale of the Aptian Stage

The age of the top of the Aptian Stage is constrained by the U-Pb age of 113.1 ± 0.3 Ma obtained on zircon crystals from the Vöhrum bentonite, approximately 100 kyr above the Aptian-Albian boundary (Selby et al., 2009; Gale et al., 2020). The astrochronology from the Valanginian to

457 the earliest Aptian in the Tethys area anchored to CA-ID-TIMS U-Pb ages in the Neuquén
458 Basin led to an age of the base of the Aptian Stage of 121.15 ± 0.31 Ma (Martinez et al., 2023).
459 Radiometric ages suggest an age of magnetochron M0r of 121.2 ± 0.5 Ma (He et al., 2008;
460 Zhang et al., 2021). Bio- and chemostratigraphic correlations suggest that magnetochron M0r
461 is equivalent in time to the *Imerites giraudi* and *Martellites sarasini* Tethyan ammonite zones
462 (Aguado et al., 2022), which age range from 122.01 to 121.15 Ma (Martinez et al., 2023). The
463 radiometric ages measured at the end of the Barremian Stage thus agree (He et al., 2008; Zhang
464 et al., 2021) with the astrochronology independently performed in the Tethys area (Martinez et
465 al., 2023). These ages constrain a duration of the Aptian Stage of 8.0 myr.

466 The astrochronology of the Piobbico core in central Italy (Huang et al., 2010) suggests the
467 existence of four or five 405-kyr eccentricity cycles from the base of the Jacob level to the top
468 of the Kilian levels implying a duration of 1.6 to 2.0 myr between these two events (Fig. 13A).
469 A shorter duration of 0.8 myr is proposed by Leandro et al. (2022) and Charbonnier et al. (2023)
470 based on the astronomical calibration of Poggio le Guaine (PLG) in Italy (Fig. 13C) and Col de
471 Pré-Guittard. Our astronomical calibration agrees best with the option of Huang et al. (2010) at
472 1.6 myr (Fig. 13B), suggesting a possible condensation/hiatus, or decreased sedimentation rate
473 not detected by Leandro et al. (2022) in this specific interval at PLG, and a decreased
474 sedimentation rate in the upper part of CPG-1 not detected in Charbonnier et al. (2023), as
475 discussed in section 5.1 (see also Figs. S1-S3 in the electronic supplement). However, the
476 duration of the whole Aptian of 13.4 myr proposed by Huang et al. (2010) does not agree with
477 the duration of 8 myr discussed above. The astrochronology of Charbonnier et al. (2023)
478 suggests a duration of 9.6 myr of the Aptian Stage assuming a duration of 0.8 myr between the
479 Jacob and Kilian events. Adding two 405-kyr eccentricity cycles would lead to a duration of
480 10.4 myr, which appears as well too long compared to the duration obtained from radiometric
481 ages.

Conversely, Leandro et al. (2022) identified 18 repetitions of the 405-kyr eccentricity cycles and estimated the duration from the Kilian Event to magnetochron M0r as 7.2 myr. Adding two repetitions of the 405-kyr cycle between the Kilian and the Jacob event to the age model of Leandro et al. (2022) leads to a duration of 8 myr from the Kilian Event to chron M0r. Anchoring this duration to the age of 113.2 Ma proposed in the Geologic Time Scale 2020 leads to an age of magnetochron M0r of 121.2 Ma, which is in falls within the radiochronology proposed by He et al. (2008). Our data thus contribute to the establishment of an increasingly precise timescale in the Aptian Stage.

Conclusions

An astronomical calibration is performed from a high-resolution magnetic susceptibility signal in the Col de Pré-Guittard section, GSSP of the Albian Stage in the Vocontian Basin, France. The section records the influence of the eccentricity and precession cycles mainly. The 405-kyr cycle is well-identified and leads to estimate a duration of the interval covering the Jacob to Leenhardt events to 4.03 myr. The duration of the Jacob-Kilian interval, Kilian-Paquier interval and Paquier-Leenhardt interval are respectively 1.55, 1.62 and 0.93 myr. The occurrence of these organic matter rich events (Jacob, Kilian, Paquier and Leenhardt) is partly controlled by the eccentricity cycle, all four events being located around the maximum of filter 405-kyr eccentricity. However, the orbital forcing on the occurrence of these events is not the sole factor explaining the onset of these events and it is likely that both volcanism and orbitally-controlled change in seasonality made the climate system to pass a threshold leading to widespread anoxia. Anchoring our timescale to the astrochronology of the Aptian of Leandro et al. (2022) and the U-Pb age of Selby et al. (2009) near the Aptian-Albian boundary, we estimate the duration from the Kilian Event to magnetochron M0r to 8 myr, and suggest an age of 121.2 Ma for

506 magnetochron M0r, which is in line with the radiometric data produced in the late Barremian
507 and magnetochron M0r.

508

Acknowledgments

The project was funded by MOPGA program (Make Our Planet Great Again), project SAD METOX from Région Bretagne, CNRS MITI Le Temps AstroCarb, and Défis Scientifiques program from Université de Rennes 1. We warmly thank Danny Boué, Anne Lise Santoni, Pierrick Roperch and Léa Beaubant for their help respectively on the field and in the laboratory. The authors are very grateful to the Editor Dr. Eduardo Koutsoukos and for the anonymous reviewers for their constructive comments, which led to improvements of the final version of the manuscript.

References

Aguado, R., Company, M., O'Dogherty, L., Sandoval, J., Martinez, M., 2022. New insights into the Barremian–lower Aptian calcareous nannofossils of the Mediterranean Tethys: Chronostratigraphic and paleobiogeographic implications. Marine Micropaleontology 173, 102114. https://doi.org/10.1016/j.marmicro.2022.102114.

Arnaud, H., Arnaud-Vanneau, A., Godet, A., Adatte, T., Massonnat, G., 2017. Barremian platform carbonates from the eastern Vercors Massif, France: Organization of depositional geometries. AAPG Bulletin 101, 485–493. https://doi.org/10.1306/011817DIG17027.

Barrier, E., Vrielynck, B., Brouillet, J.-F., Brunet, M.-F., 2018. Paleotectonic Reconstruction of the of the Central Tethyan Realm. CCGM-CGMW, Paris.

Benamara, A., Charbonnier, G., Adatte, T., Spangenberg, JE., Föllmia, KB., 2020. Precession-driven monsoonal activity controlled the development of the early Albian Paquier oceanic anoxic event (OAE1b): Evidence from the Vocontian Basin, SE France. Palaeogeography, Palaeoclimatology, Palaeoecology 537, 109406. https://doi.org/10.1016/j.gloplacha.2022.103959.

Bodin, S., Meissner, P., Janssen, N. M., Steuber, T., Mutterlose, J., 2015. Large igneous provinces and organic carbon burial: Controls on global temperature and continental weathering during the Early Cretaceous. Global and Planetary Change 133, 238–253. https://doi.org/10.1016/j.gloplacha.2015.09.001.

Bodin, S., Charpentier, M., Ullmann, C.V., Rudra, A., Sanei, H. Carbon cycle during the late Aptian-deposits Albian OAE 1b : A focus on the Kilian-Paquier levels interval. Global and Planetray Change 222, 104074. https://doi.org/10.1016/j.gloplacha.2023.104074.

Bottini, C., and Erba, E., 2018. Mid-Cretaceous paleoenvironmental changes in the western Tethys. Climate of the Past Discussions, 1–23. https://doi.org/10.5194/cp-14-1147-2018.

Bottini, C., Erba, E., Tiraboschi, D., Jenkyns, HC., Schouten, S., Sinninghe Damsté, JS., 2015. Climate variability and ocean fertility during the Aptian Stage. Climate of the Past 11, 383–402. https://doi.org/10.5194/cp-11-383-2015.

Bracquart, E., Charbonnier, G., Garel, S., Munier, T., Adatte, T., Danzelle, J., 2022. New evidences of subaerial volcanism as a trigger for the Kilian event (Aptian-Albian transition) and major climatic changes from offshore Morocco (DSDP Site 545). Global and Planetary Change 218, 103959. https://doi.org/10.1016/j.gloplacha.2022.103959.

Bréhéret, J.G., 1985. Indices d'un événement anoxique étendu à la Téthys alpine, à l'Albien inférieur (événement Paquier). C.R. Acad. Sci., Paris 300, II, 8, 355–358.

Bréhéret, J.G., 1988. Episodes de sédimentation riche en matière organique dans les marnes bleues d'âge Aptien et Albien de la partie pélagique du bassin Vocontien. Bull. Soc. Géol. Fr. 8, 349–356. https://doi.org/10.2113/gssgfbull.IV.2.349.

Bréhéret, J.G., 1997. L'Aptien et l'Albien de la Fosse vocontienne (des bordures au bassin). Évolution de la sédimentation et enseignements sur les événements anoxiques. Société géologique du Nord 25, 644.

Bréhéret, J.G and Brumsack, H-J., 2000. Barite concretions as evidence of pauses in sedimentation in the Marnes Bleues Formation of the Vocontian Basin (SE France). Sedimentary Geology 130, 205–228. https://doi.org/10.1016/S0037-0738(99)00112-8.

Caillaud, A., Quijada, M., Hlohowskyj, SR., Chappaz, A., Bout-Roumazeilles, V., Reynaud, J-Y., Riboulleau, A., Baudin, F., Adatte, T., Ferry, J-N., Tribovillard, N., 2022. Assessing controls on organic matter enrichments in hemipelagic marls of the Aptian-Lower Albian Blue Marls of the Vocontian Basin (France): an unexpected variability observed from multiple "organic-rich" levels. BSGF – Earth Sciences Bulletin 193, 2. https://doi.org/10.1051/bsgf/2022001.

Charbonnier, G., Boulila, S., Spangenberg, J.E., Vermeulen, J., Galbrun, B., 2023. Astrochronology of the Aptian stage and evidence for the chaotic motion of Mercury. Earth and Planetary Science Letters 610, 118104. https://doi.org/10.1016/j.epsl.2023.118104.

Cleveland, W.S., 1979. Robust Locally Regression and Smoothing Scatterplots. Journal of American Statistical Association 74, 829–836.

Coccioni, R., Sabatino, N., Frontalini, F., Gardin, S., Sideri, M., Sprovieri, M., 2014. The neglected history of Oceanic Anoxic Event 1b: insights and new data from the Poggio le Guaine section (Umbria–Marche Basin). Stratigraphy 11, 245–282.

Coffin, M.F., Pringle, M.S., Duncan, R.A., Gladczenko, T.P., Storey, M., Müller, R.D., and Gahagan, L.A., 2002, Kerguelen hotspot magma output since 130 Ma. Journal of Petrology 43, 1121–1137. https://doi.org/10.1093/petrology/43.7.1121.

Corentin, P., Deconinck, J.F., Pellenard, P., Amédro, F., Bruneau, L., Chenot, E., Matrion, B., Huret, E., Landrein, P., 2020. Environmental and climatic controls of the clay mineralogy of Albian deposits in the Paris and Vocontian Basins (France). Cretaceous Research 108, 104342. https://doi.org/10.1016/j.cretres.2019.104342.

Dercourt, J., Ricou, L.E., Vrielynck, B., 1993. Atlas Tethys Paleoenvironmental Maps. Gauthier-Villars, Paris.

Erba, E., 1994. Nannofossils and superplumes. The early Aptian 'nannoconid crisis'. Paleoceanography 9, 483–501. https://doi.org/10.1029/94PA00258.

Erbacher, J., Hemleben, C., Huber, B.T., Markey, M., 1999. Correlating environmental changes during early Albian oceanic anoxic event 1B using benthic foraminiferal paleoecology. Marine Micropaleontology 38, 7–28. https://doi.org/10.1016/S0377-8398(99)00036-5.

Erbacher, J. and Thurow, J., 1997. Influence of oceanic anoxic events on the evolution of mid-Cretaceous radiolaria in the North Atlantic and western Tethys. Mar. Micropaleontol 30, 139–158. https://doi.org/10.1016/S0377-8398(96)00023-0.

Föllmi, K.B., 2012. Early Cretaceous life, climate and anoxia. Cretaceous Research 35, 230–257. https://doi.org/10.1016/j.cretres.2011.12.005.

Friedrich,O., 2010. Benthic foraminifera and their role to decipher paleoenvironment during mid-Cretaceous Oceanic Anoxic Events -the "anoxic benthic foraminifera" paradox. Revue de micropaléontologie 53, 175–192. https://doi.org/10.1016/j.revmic.2009.06.001.

Friès, G. and Parize, O., 2003. Anatomy of ancient passive margin slope systems: Aptian gravity-driven deposition on the Vocontian palaeomargin, western Alps, south-east France. Sedimentology 50, 1231–1270. https://doi.org/10.1111/j.1365-3091.2003.00601.x.

Gale, A. S., Mutterlose, J., Batenburg, S. In Geologic Time Scale 2020 (eds Gradstein, F. M. et al.) 1023–1068. https://doi.org/10.1016/B978-0-12-824360-2.00027-9.

Ghirardi, J., Deconinck, J.F., Pellenard, P., Martinez, M., Bruneau, L., Amiotte- Suchet, P., Pucéat, E., 2014. Multi-proxy orbital chronology in the aftermath of the Aptian Oceanic Anoxic Event 1a: Palaeoceanographic implications (Serre Chaitieu section, Vocontian Basin, SE France). Newsletters on Stratigraphy 47, 247–262. https://10.1127/0078-0421/2014/0046.

He, H., Pan, Y., Tauxe, L., Qin, H., Zhu, R., 2008. Toward age determination of the M0r (Barremian–Aptian boundary) of the early Cretaceous. Phys. Earth Planet. Inter. 169, 41–48. https://doi.org/10.1016/j.pepi.2008.07.014.

603 Heimhofer, U., Hochuli, P.A., Herrle, J.O., Andersen, N., Weissert, H., 2004. Absence of major vegetation and
604 palaeoatmospheric pCO2 changes associated with oceanic
605 anoxic event 1a (early Aptian, SE France). Earth and Planetary Science Letters 223, 303–318.
606 https://doi.org/10.1016/j.epsl.2004.04.037.
607 Herrle, J.O., and Mutterlose, J., 2003. Calcareous nannofossils from Aptian–Lower Albian of southeast France:
608 palaeoecological and biostratigraphic implications: Cretaceous Research 24, 1–22.
609 https://doi.org/10.1016/S0195-6671(03)00023-5.

610 Herrle, J.O., Kößler, P., Friedrich, O., Erlenkeuser, H., Hemleben, C., 2004. High-resolution carbon isotope
611 records of the Aptian to Lower Albian from SE France and the Mazagan Plateau (DSDP site 545): a
612 stratigraphic tool for paleoceanographic and paleobiologic reconstruction, Earth and Planetary Science
613 Letters 218, 149–161. https://doi.org/10.1016/S0012-821X (03)00646-0.

614 Herrle, J.O., Schröder-Adams, C.J., Davis, W., Pugh, A.T., Galloway, J.M., Fath, J., 2015. Mid- Cretaceous igh
615 Arctic stratigraphy, climate, and Oceanic anoxic events. Geology 43, 403–406.
616 https://doi.org/10.1130/G36439.1.
617
618 Huang, C., Hinnov, L., Fischer, A.G., Grippo, A., Herbert, T., 2010. Astronomical tuning of the Aptian Stage from
619 Italian reference sections. Geology 30, 899–902. https://doi.org/10.1130/G31177.1.

620 Huber, B.T., Leckie, R.M., 2011. Planktic foraminiferal turnover across deep-sea Aptian/Albian boundary
621 sections. Journal of Foraminiferal Research 41, 53–95. https://doi.org/10.2113/gsjfr.41.1.53.

622 Jovane, L., Florindo, F., Sprovieri, M., P¨ alike, H., 2006. Astronomic calibration of the late Eocene/early
623 Oligocene Massignano section (Central Italy). Geochem. Geophys. Geosyst. 7, 1–10.
624 https://doi.org/10.1029/2005GC001195.

625 Kennedy, W.J., Gale, A.S., Bown, P.R., Caron, M., Davey, R.J., Gröcke, D., and Wray, D.J., 2000. Integrated
626 stratigraphy across the Aptian–Albian boundary in the Marnes Bleues, at the Col de Pré-Guittard,
627 Arnayon (Drôme), and at Tartonne (Alpes-de-Haute-Provence), France, a candidate Global boundary
628 Stratotype Section and Point for the base of the Albian Stage. Cretaceous Research 21, 591–720.
629 https://doi.org/10.1006/cres.2000.0223.

630 Kennedy, J.W., Gale, A.S., Huber, B.T., Petrizzo, M.R., Bown, P., Jenkyns, H.C., 2017. The Global Boundary
631 Stratotype Section and Point (GSSP) for the base of the Albian Stage, of the Cretaceous, the Col de Pré-
632 Guittard section, Arnayon, Drôme, France. Episodes 40, 177–188.
633 https://doi.org/10.18814/epiiugs/2017/v40i3/017021.

634 Kößler, P., Herrle, JO., Appel, E., Erbacher, J., Hemleben, C., 2001. Magnetic records of climatic cycles from
635 mid-cretaceous hemipelagic sediments of the Vocontian Basin, SE France. Cretaceous Research 22,
636 321–331. https://doi.org/10.1006/cres.2001.0256.

637 Laskar, J., Robutel, P., Joutel, F., Gastineau, M., Correia, A.C.M., Levrard, B., 2004. A long-term numerical
638 solution for the insolation quantities of the Earth. Astron. Astrophys. 428, 261–285.
639 https://doi.org/10.1051/0004-6361:20041335.

640 Leandro, C.G., Savian, J.F., Kochhann, M.V.L., Franco, D.R., Coccioni, R., Frontalini, F., Gardin, S., Jovane, L.,
641 Figueiredo, M., Tedeschi, L.R., Janikan, L., Almeida, R. P., Trindade, R. P. F., 2022. Astronomical
642 tuning of the Aptian stage and its implications for age recalibrations and paleoclimatic events. Nat
643 Commun 13, 2941. https://doi.org/10.1038/s41467-022-30075-3.

644

645 Li, M., Hinnov, L., Kump, L., 2019. Acycle: Time-series analysis software for paleoclimate research and eduction.
646 Computers & Geosciences 127, 12-22.

647 Mann, M.E., Lees, J.M., 1996. Robust estimation of background noise and signal detection in climatic time series.
648 Clim. Change 33, 409–445. https://doi.org/10.1007/BF00142586.

649 Martinez, M., Aguirre-Urreta, B., Dera, G., Lescano, M., Omarini, J., Tunik, M., O'Dogherty, L., Aguado, R.,
650 Company, M., Bodin, S., 2023. Synchrony of carbon cycle fluctuations, volcanism and orbital forcing
651 during the Early Cretaceous. Earth-Science Reviews 239, 104356.
652 https://doi.org/10.1016/j.earscirev.2023.104356.

Martinez, M., Deconinck, J.F., Pellenard, P., Riquier, L., Company, M., Reboulet, S., Moiroud, M., 2015. Astrochronology of the Valanginian–Hauterivian stages (Early Cretaceous): chronological relationships between the Paraná–Etendeka large igneous province, the Weissert and the Faraoni events. Glob. Planet. Change 131, 158–173. https://doi.org/10.1016/j.gloplacha.2015.06.001.

Matsumoto, H., Kuroda, J., Coccioni, R., Frontalini, F., Sakai, S., Ogawa, N.O., Ohkouchi, N., 2020. Marine Os isotopic evidence for multiple volcanic episodes during Cretaceous Oceanic Anoxic Event 1b. Sci. Rep. 10, 12601. https://doi.org/10.1038/s41598-020-69505-x.

McAnena, A., Flögel, S., Hofmann, P., Herrle, J.O., Griesand, A., Pross, J., Talbot, H.M., Rethemeyer, J., Wallmann, K., Wagner, T., 2013. Atlantic cooling associated with a marine biotic crisis during the mid-Cretaceous period Nat. Geosci. 6 , 558–561. https://doi.org/10.1038/ngeo1850.

Millán, M.I., Weissert, H.J., López-Horgue, M.A., 2014. Expression of the late Aptian cold snaps and the OAE1b in a highly subsiding carbonate platform (Aralar, Northern Spain). Palaeogeogr. Palaeoclimatol. Palaeoecol., 411,167–179. https://doi.org/10.1016/j.palaeo.2014.06.024.

Mutterlose, J., Bornemann, A., Herrle, J., 2009. The Aptian–Albian cold snap: evidence for "mid" Cretaceous icehouse interludes. N. Jb. Geol. Paläont. 252, 217–225. 10.1127/0077-7749/2009/0252-0217.

Price, G.D., 1999. The evidence and implications of polar ice during the Mesozoic. Earth Sci. Rev. 48, 183–210. https://doi.org/10.1016/S0012-8252(99)00048-3.

Rodríguez-López, J-p., C-L., Pardo, G., Meléndez, N., Soria A-R., Skillinga, I., 2016. Glacial dropstones in the western Tethys during the late Aptian–early Albian cold snap: Palaeoclimate and palaeogeographic implications for the mid-Cretaceous. Palaeogeography,Palaeoclimatology, Palaeoecology, 452, 11–27. https://doi.org/10.1016/j.palaeo.2016.04.004.

Prokopenko, A.A., Hinnov, L.A., Williams, D.F., Kuzmin, M.I., 2006. Orbital forcing of continental climate during the Pleistocene: a complete astronomically tuned climatic record from Lake Baikal, SE Siberia. Quaternary Science Reviews 25, 3431–3457. https://doi.org/10.1016/j.quascirev.2006.10.002.

Sabatino, N., Ferraro, S., Coccioni, R., Bonsignore, M., Del, M., Tancredi, V., et al. 2018. Mercury anomalies in upper Aptian-lower Albian sediments from the Tethys realm. Palaeogeography, Palaeoclimatology, Palaeoecology 495, 163–170. https://doi.org/10.1016/j.palaeo.2018.01.008.

Selby, D., Mutterlose, J., and Condon, D.J., 2009. U-Pb and Re-Os Geochronology of the Aptian/Albian and Cenomanian/Turonian stage boundaries: implications for timescale calibration, osmium isotope seawater composition and Re-Os systematics in organic-rich sediments. Chemical Geology 265, 394–409. https://doi.org/10.1016/j.chemgeo.2009.05.005.

Thomson, D. J. 1982., Spectrum estimation and harmonic analysis, P. IEEE 70, 1055–1096. https://0018-9219/82/0900-1055.

Thomson, D. J., 1990., Quadratic-Inverse Spectrum Estimates: Applications to Palaeoclimatology, Philos. T. R. Soc. Lond. A., 332, 539–597. https://doi.org/10.1098/rsta.1990.0130.

Wagner, T., Herrle, J.O., Sinninghe Damsté, J.S., Schouten, S., Stüsser, I., Hofmann, P., 2008. Rapid warming and salinity changes of Cretaceous surface waters in the subtropical North Atlantic. Geology 36, 203–206. https://doi.org/10.1130/G24523A.1.

Wang, Y., Bodin, S., Blusztajn, J.S., Ullmann, C., and Nielsen, S.G., 2022, Orbitally paced global oceanic deoxygenation decoupled from volcanic CO2 emission during the middle Cretaceous Oceanic Anoxic Event 1b (Aptian-Albian transition): Geology, 50, 1324–1328. https://doi.org/10.1130/G50553.1.

Wilpshaar, M., Leereveld, H., 1994. Palaeoenvironmental change in the Early Cretaceous Vocontian Basin (SE France) reflected by dinoflagellate cysts. Review of Palaeobotany and Palynology 84. 121-128. https://10.1016/0034-6667(94)90046-9.

Zhang, Y., Ogg, J.G., Minguez, D., Hounslow, MW., Olaussen, S., Gradstein, F, M., Esmeray-Senlet, S., 2021. Magnetostratigraphy of U-Pb–dated boreholes in Svalbard, Norway, implies that magnetochron M0r (a proposed Barremian-Aptian boundary marker) begins at 121.2 ± 0.4 Ma. Geology 49. 733–737. https://doi.org/10.1130/G48591.1.

Figures captions:

Fig. 1. Location, paleogeography, and pictures of the Col de Pré-Guittard section. A. Location of the Col de Pré-Guittard section within the Vocontian Basin (from Friès and Parize 2003). B. Palaeogeography of the Central-North Atlantic during the Aptian with the location of the Vocontian Basin (Barrier et al. 2018). C. Overview of Col de Pré-Guittard 2 (CPG2). D. Close-up view of the Paquier Level.

Fig. 2. Detailed location of the two sections of Col Pré-Guittard (CPG). A. Simplified Geographic map of Col de Pré-Guittard region showing the two studied sections, the map provided from the Institut Géographique National (France) available at infoterre.brgm.fr. The brown circles indicate the locations of the sections and the black rectangle corresponds to the area shown in (B). B. Aerial photography of the Col de Pré-Guittard, area available at https://www.geoportail.gouv.fr/.

Fig. 3. Long-term evolution of geochemical proxies along the CPG-1 and CPG-2. A. Stratigraphic evolution of the Magnetic susceptibility (MS, $x10^{-8}$ m^3. kg^{-1}) records from the CPG-1. B. Magnetic susceptibility (MS, $x10^{-8}$ **m^3/kg**) records from the CPG-2. From C to F. Trend evolution of total organic carbon (TOC, wt.%), hydrogen index (HI, mgHC/g TOC), oxygen index (OI, $mgCO_2$/g TOC) and $\delta^{13}C_{org}$ (‰ VPDB) records respectively from CPG-2. The light brown color defines the position of the four events (Jacob, Kilian, Paquier and Leenhardt) and the red line corresponds to the long-term trend of the series in different proxies.

Fig. 4. Cross plots of the magnetic susceptibility vs carbonate contents for CPG-2. The red line represents the linear regression with the correlation coefficients.

Fig.5: Stratigraphic evolution of TOC, HI and $\delta^{13}C_{org}$ along Col de Pré Guittard (this study) compared to Les Briers section, data are from Bodin et al. (2023).

Fig. 6. 2π Multi-Taper Method (MTM) spectra with Coefficient Correlation COCO analysis for CPG-1. Periods are labelled in meters in the spectral peaks and labeled with different colors, red for 405-kyr eccentricity, orange for 100-kyr eccentricity, and green for obliquity and blue for 20-kyr precession.

Fig. 7. Spectral analyses and astrochronology of the CPG-1. A. Raw MS signal. B. Filters of the 405-kyr band (red color) and the 100-kyr band (orange color). C. Amplitude spectrograms performed on 25-m width windows. D. Amplitude spectrograms performed on 10-m width windows after filtering the lowest frequencies. E. H0 significance levels at sedimentation rates ranging from 0.7 to 6 cm/kyr calculated with the eCOCO procedure performed on 25-m width windows.

Fig. 8. 2π Multi-Taper Method (MTM) with Coefficient Correlation COCO analysis for the CPG2. Periods are labelled in meters with different colors, red for 405-kyr eccentricity, orange for 100-kyr eccentricity, and green for obliquity and blue for 20-kyr precession.

Fig. 9. Spectral analyses of CPG-2. A. Raw MS signal. B. Filters of the 405-kyr band (red color) and the 100-kyr band (orange color). C. Amplitude spectrograms performed on 40-m width windows. D. Amplitude spectrograms performed on 15-m width windows. E. H0 significance level at sedimentation rates ranging from 0.7 to 10 cm/kyr calculated with the eCOCO procedure performed on 40-m width windows

Fig.10: Revised spectral analysis was conducted on the Col de Pré Guittard section using data provided by Charbonnier et al. (2023). A. Raw magnetic susceptibility data is represented in black, while the long-term evolution is shown in red. B and C displays spectrograms with windows sizes of 60 m and 15 m, respectively. The significant periods are labeled in meters. D and E demonstrate the H0 significance level calculated from eCOCO analysis, performed on width windows at 60 m and 25 m, respectively, indicating the mean average sedimentation rate.

F, G, and H present the 2π-Multi-Taper Method (MTM) spectra conducted on three subdivided intervals: interval 1 (from the base of the series to 320 m), interval 2 (from 315 m to 365 m), and finally, interval 3 (from 360 m to the top of the series).

Fig. 11. An overview of the astronomical calibration of Col de Pré Guittard section (CPG 2) correlated to the recent data provided from les Briers section, $CaCO_3$ data are from Bodin et al. (2023). A. Raw MS signal. B. Filters of the 405-kyr band (red color) and the 100-kyr band (orange color) C. Raw $CaCO_3$ while the long-term evolution is shown in red. D. Filter of the 405-kyr band (red color).

Fig. 12. 2π Multi-Taper Method (MTM) analysis performed on $CaCO_3$ carbonate content from Les Briers section, data provided from Bodin et al. (2023).

Fig. 13. Correlations of astronomical time scale for the Jacob-Kilian interval in Piobbico core, Central Italy (Huang et al. 2010) and Col de Pré-Guittard section, Vocontian basin (present study), and Poggio le Guanine core (Leandro et al. 2022).

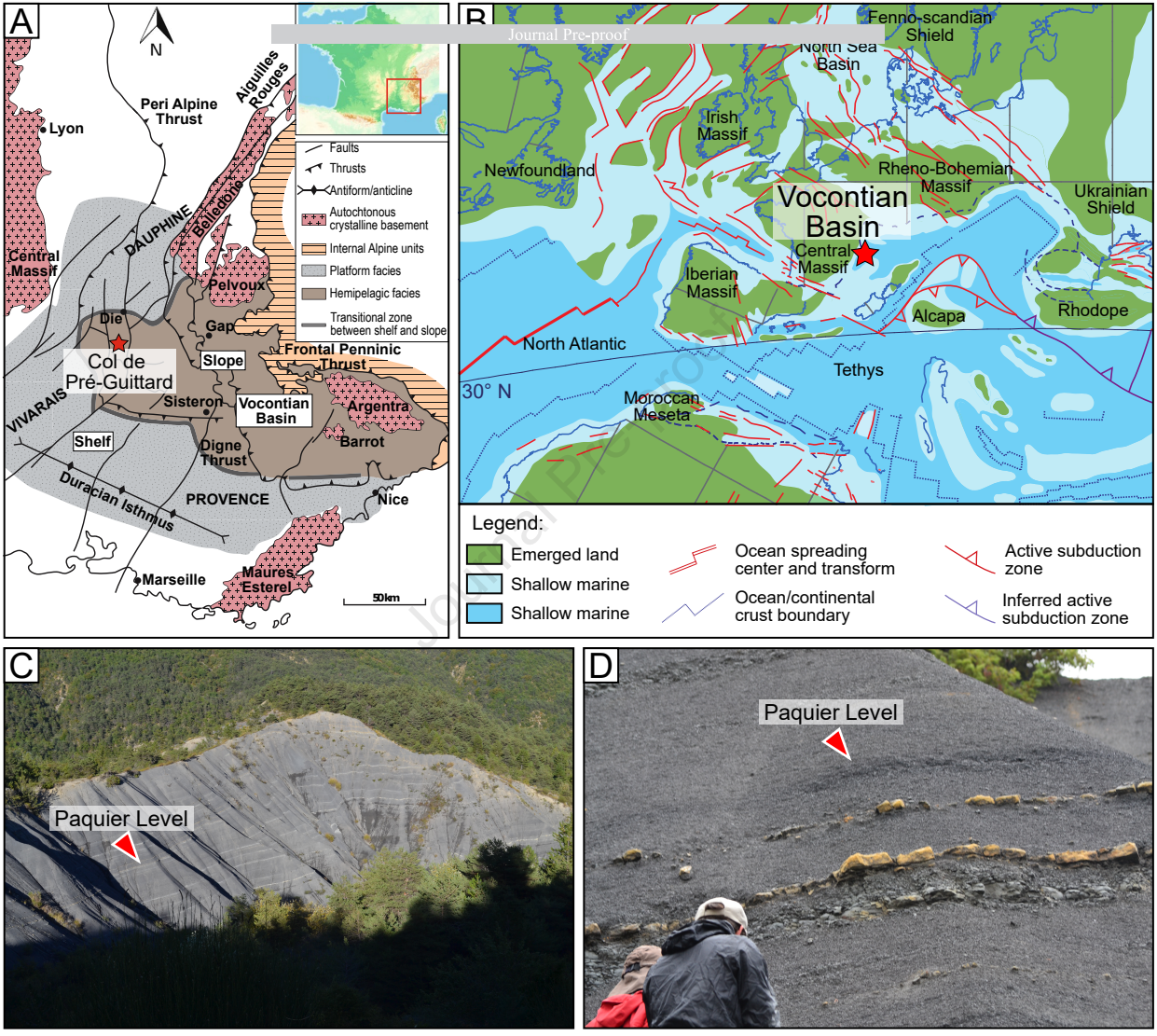
A
N
Peri Alpine Thrust
Aiguilles Rouges
Lyon
Faults
Thrusts
Antiform/anticline
Autochtonous crystalline basement
Internal Alpine units
Platform facies
Hemipelagic facies
Transitional zone between shelf and slope
Central Massif
DAUPHINE
Belledonne
Pelvoux
Die
Gap
Col de Pré-Guittard
Slope
Frontal Penninic Thrust
VIVARAIS
Sisteron
Vocontian Basin
Argentra
Shelf
Digne Thrust
Barrot
Durancian Isthmus
PROVENCE
Nice
Marseille
Maures Esterel
50km
B
Journal Pre-proof
Fenno-scandian Shield
North Sea Basin
Irish Massif
Newfoundland
Rheno-Bohemian Massif
Ukrainian Shield
Vocontian Basin
Central Massif
Iberian Massif
Alcapa
Rhodope
North Atlantic
Tethys
30° N
Moroccan Meseta
Legend:
Emerged land
Shallow marine
Shallow marine
Ocean spreading center and transform
Ocean/continental crust boundary
Active subduction zone
Inferred active subduction zone
C
Paquier Level
D
Paquier Level

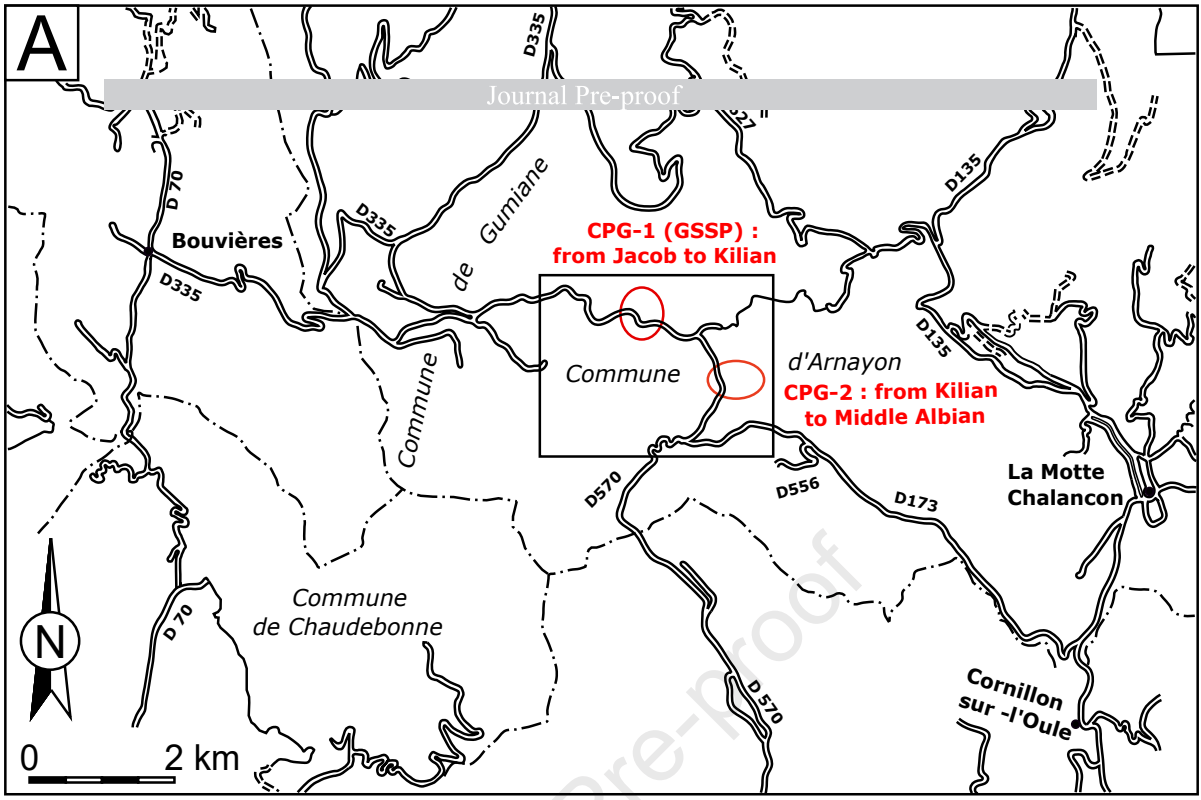

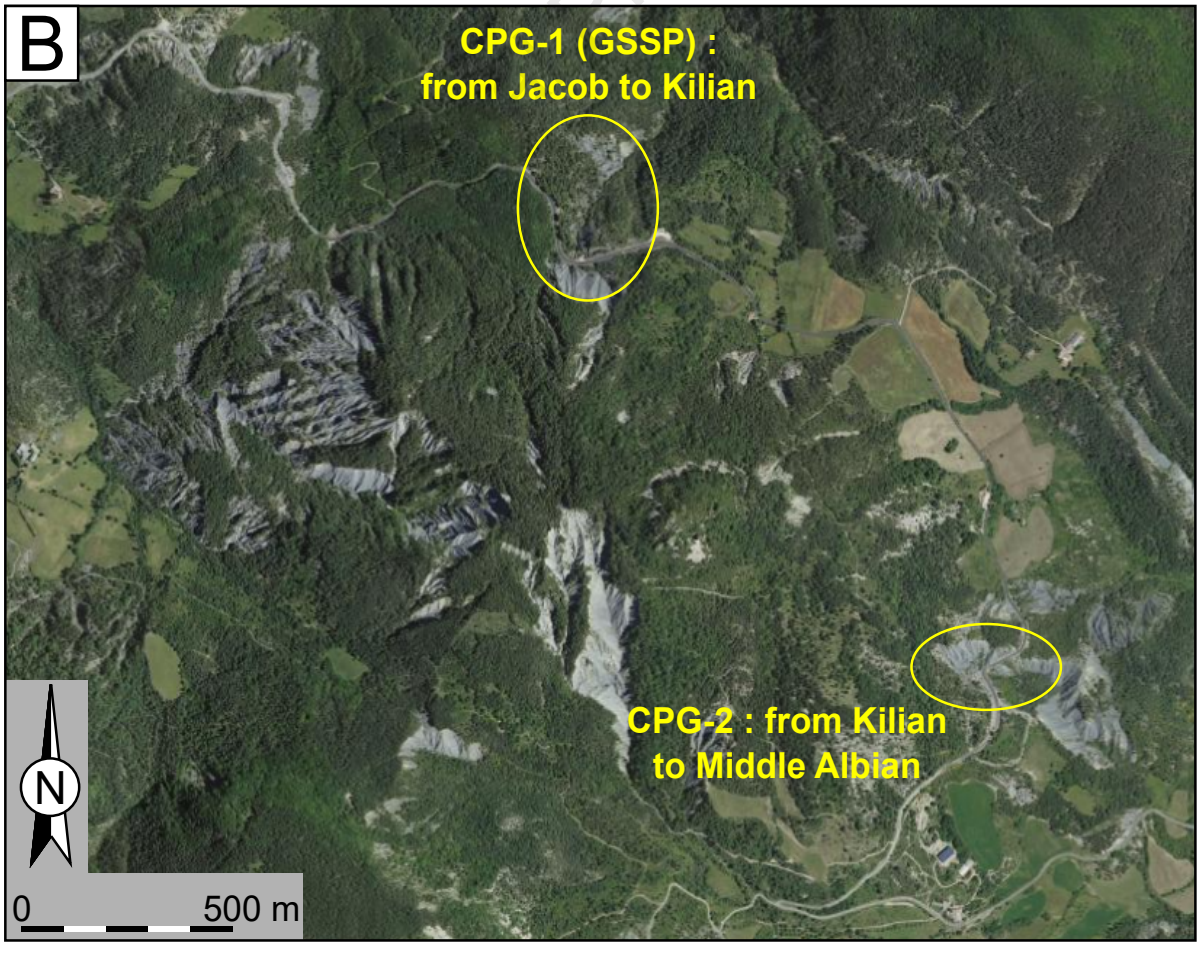

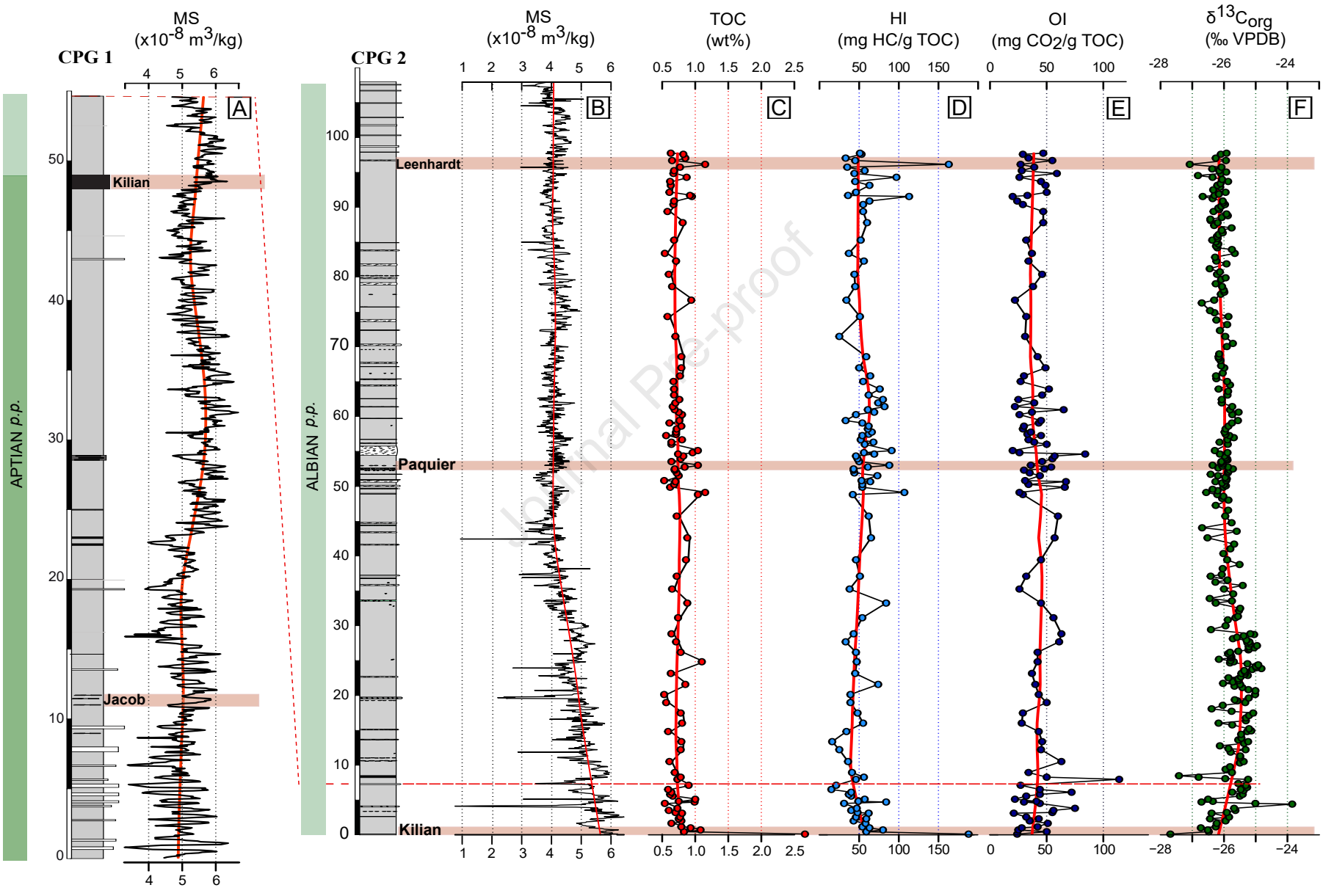

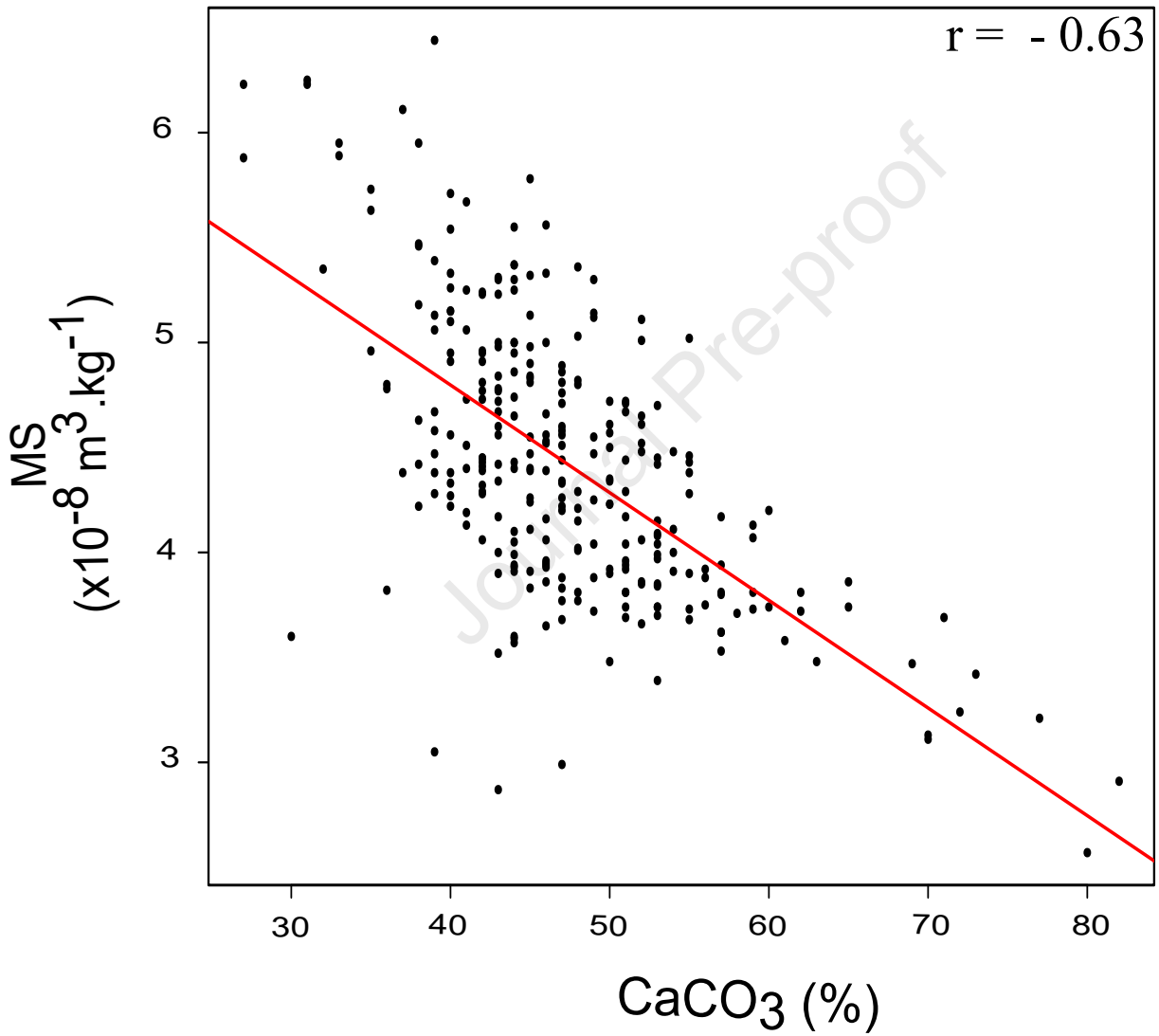

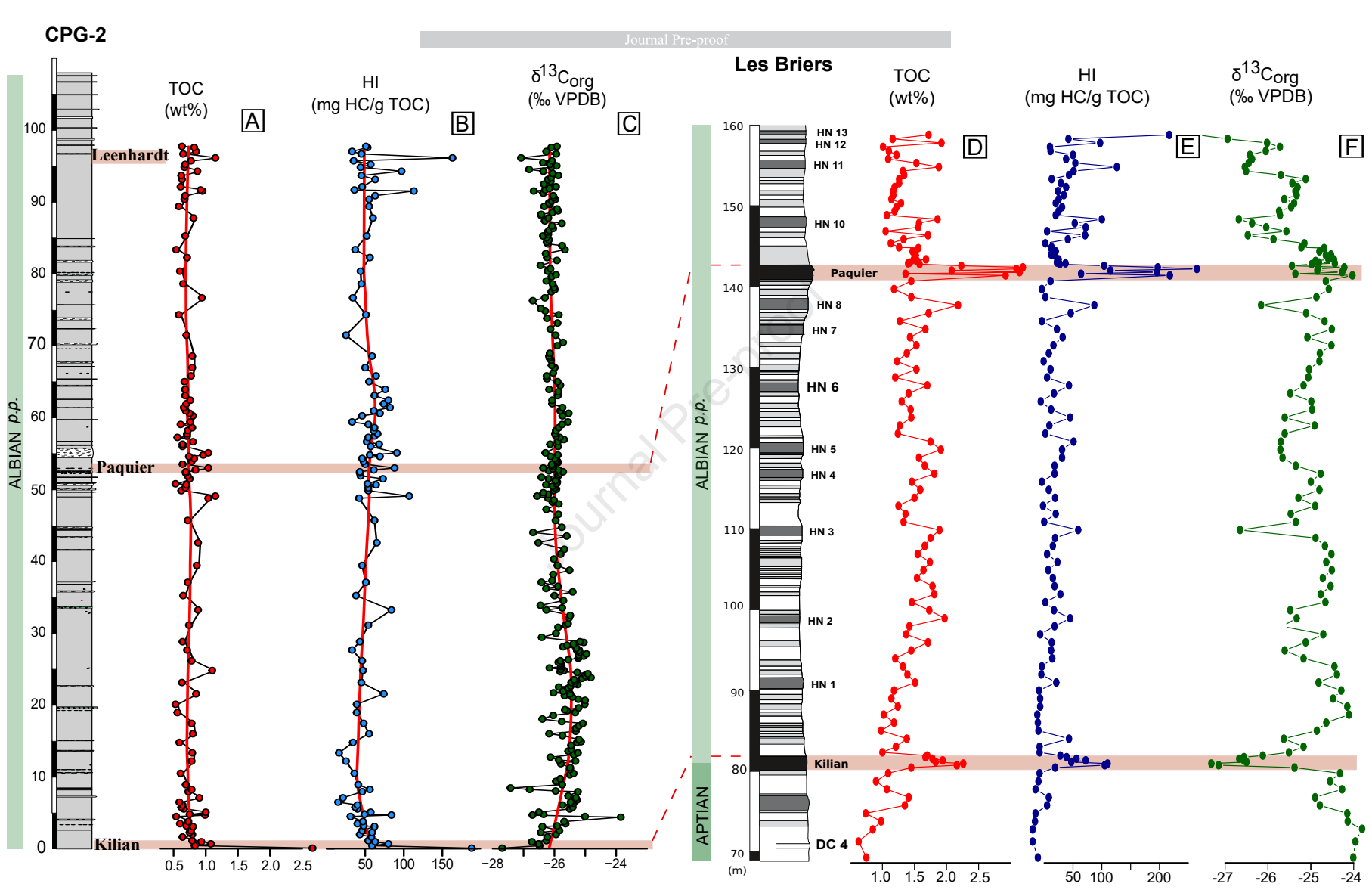

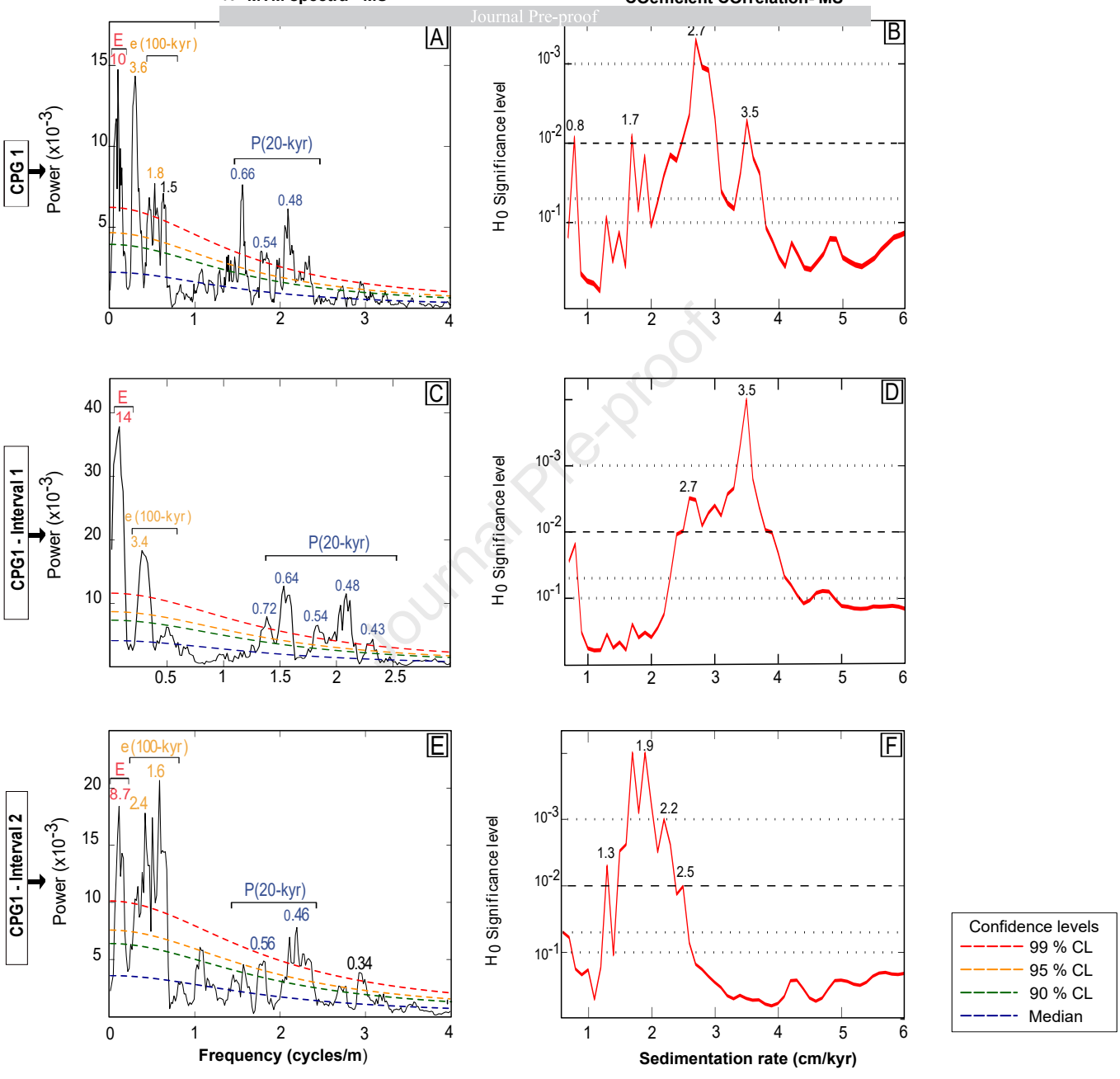
2 π-MTM spectra - MS
COefficient COrrelation- MS
Journal Pre-proof
A
B
C
D
E
F
CPG 1
CPG1 - Interval 1
CPG1 - Interval 2
Power (x10-3)
H0 Significance level
E
10
3.6
e (100-kyr)
1.8
1.5
P(20-kyr)
0.66
0.48
0.54
0.8
1.7
2.7
3.5
14
3.4
0.64
0.72
0.54
0.48
0.43
8.7
2.4
1.6
0.46
0.56
0.34
1.9
2.2
1.3
2.5
Frequency (cycles/m)
Sedimentation rate (cm/kyr)
Confidence levels
99 % CL
95 % CL
90 % CL
Median

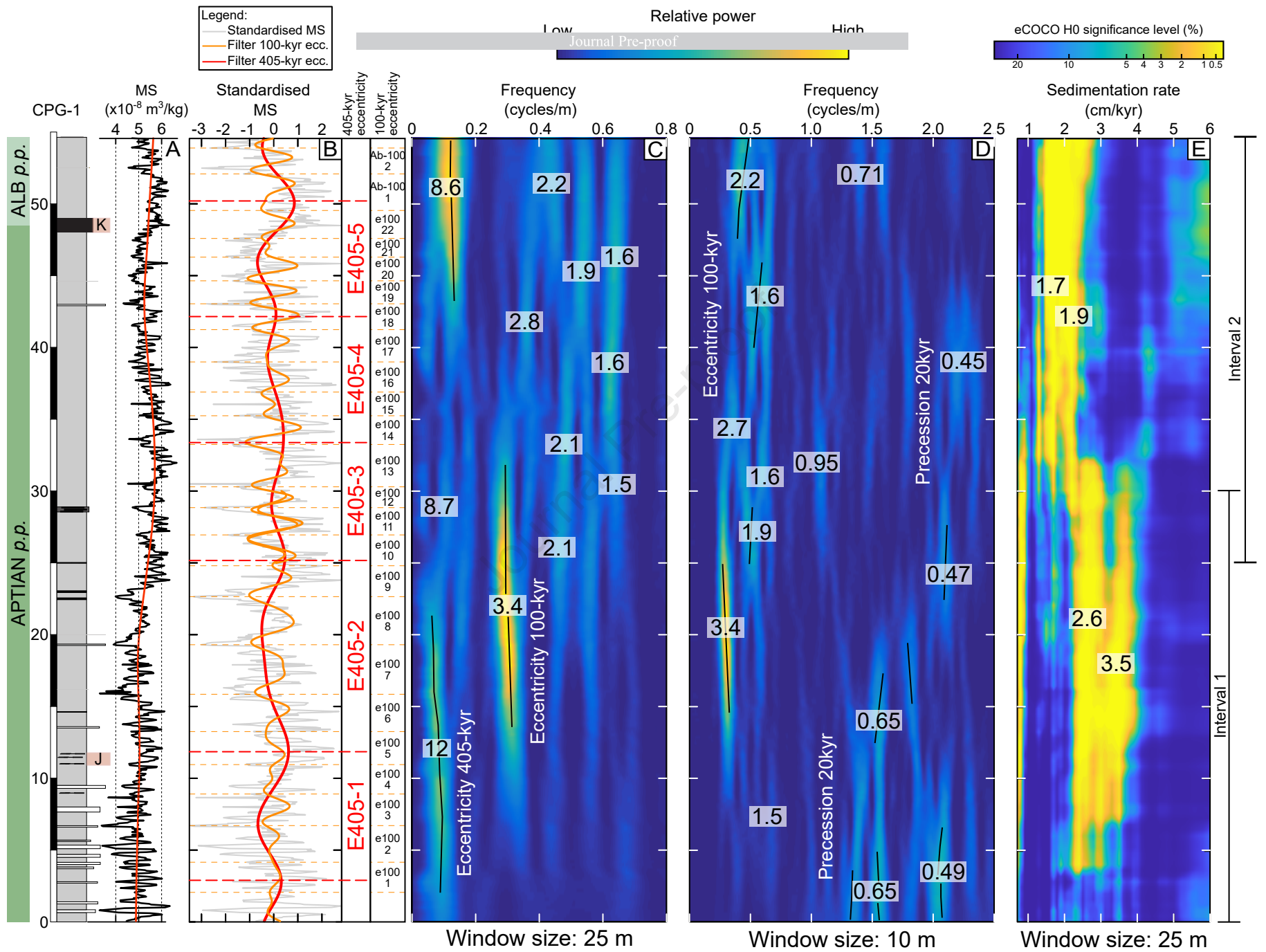
Legend:
Standardised MS
Filter 100-kyr ecc.
Filter 405-kyr ecc.
Relative power
Low
High
Journal Pre-proof
eCOCO H0 significance level (%)
20
10
5
4
3
2
1
0.5
CPG-1
MS (x10-8 m3/kg)
Standardised MS
405-kyr eccentricity
100-kyr eccentricity
Frequency (cycles/m)
Frequency (cycles/m)
Sedimentation rate (cm/kyr)
A
B
C
D
E
ALB p.p.
APTIAN p.p.
K
J
E405-5
E405-4
E405-3
E405-2
E405-1
Eccentricity 405-kyr
Eccentricity 100-kyr
Eccentricity 100-kyr
Precession 20kyr
Precession 20kyr
Interval 2
Interval 1
Window size: 25 m
Window size: 10 m
Window size: 25 m

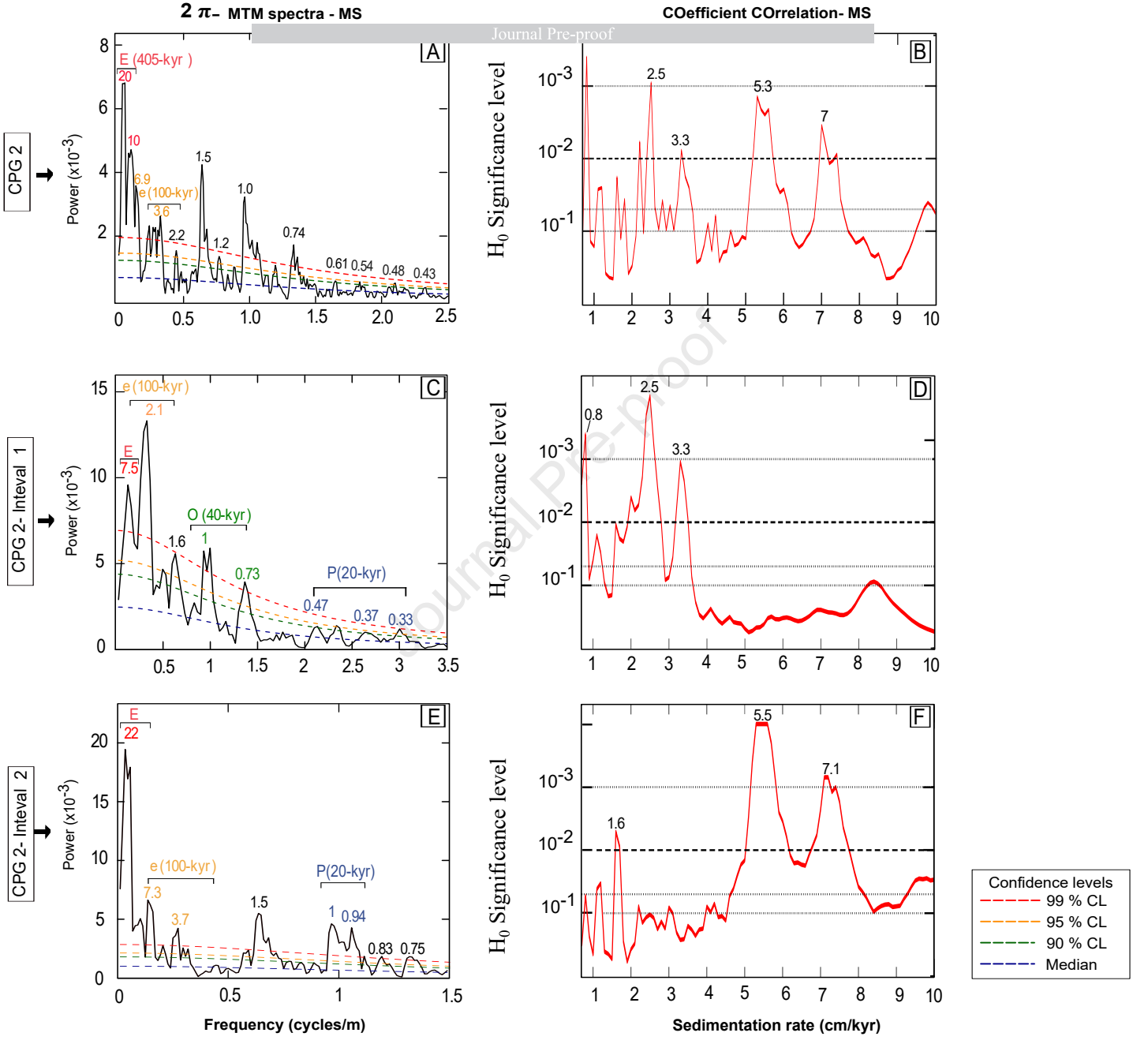

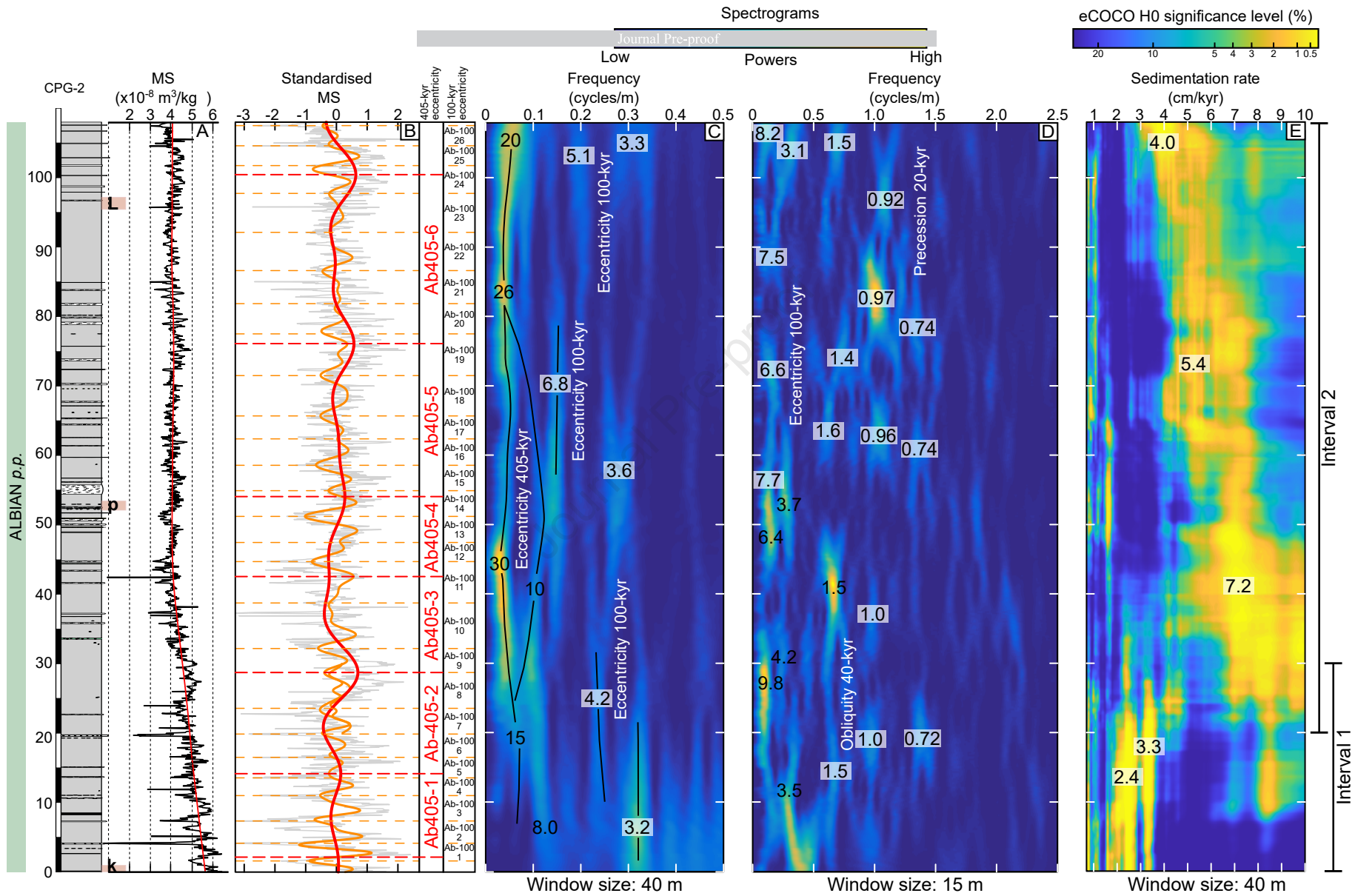
Spectrograms
Journal Pre-proof
Low
Powers
High
eCOCO H0 significance level (%)
20 10 5 4 3 2 1 0.5
CPG-2
MS
(x10-8 m3/kg)
Standardised
MS
405-kyr
eccentricity
100-kyr
eccentricity
Frequency
(cycles/m)
Sedimentation rate
(cm/kyr)
A
B
C
D
E
ALBIAN p.p.
Ab405-6
Ab405-5
Ab405-4
Ab405-3
Ab405-2
Ab405-1
Eccentricity 100-kyr
Eccentricity 405-kyr
Precession 20-kyr
Obliquity 40-kyr
Interval 2
Interval 1
Window size: 40 m
Window size: 15 m
Window size: 40 m

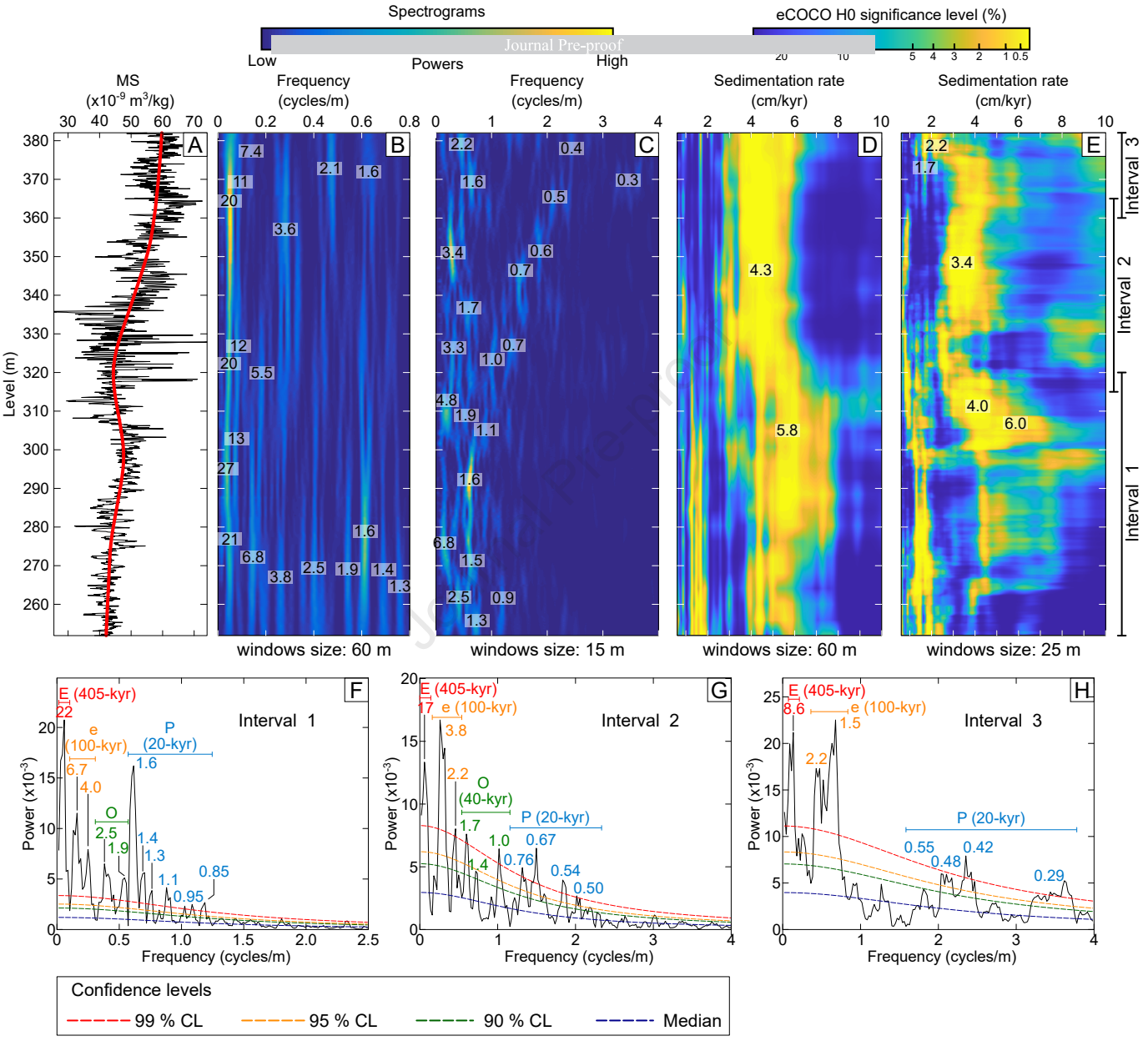
Spectrograms
Low
Powers
High
eCOCO H0 significance level (%)
20
10
5
4
3
2
1
0.5
MS
(x10-9 m3/kg)
Frequency
(cycles/m)
Sedimentation rate
(cm/kyr)
Level (m)
A
B
C
D
E
Interval 3
Interval 2
Interval 1
windows size: 60 m
windows size: 15 m
windows size: 60 m
windows size: 25 m
F
G
H
E (405-kyr)
e
(100-kyr)
P
(20-kyr)
O
(40-kyr)
Power (x10-3)
Frequency (cycles/m)
Confidence levels
99 % CL
95 % CL
90 % CL
Median

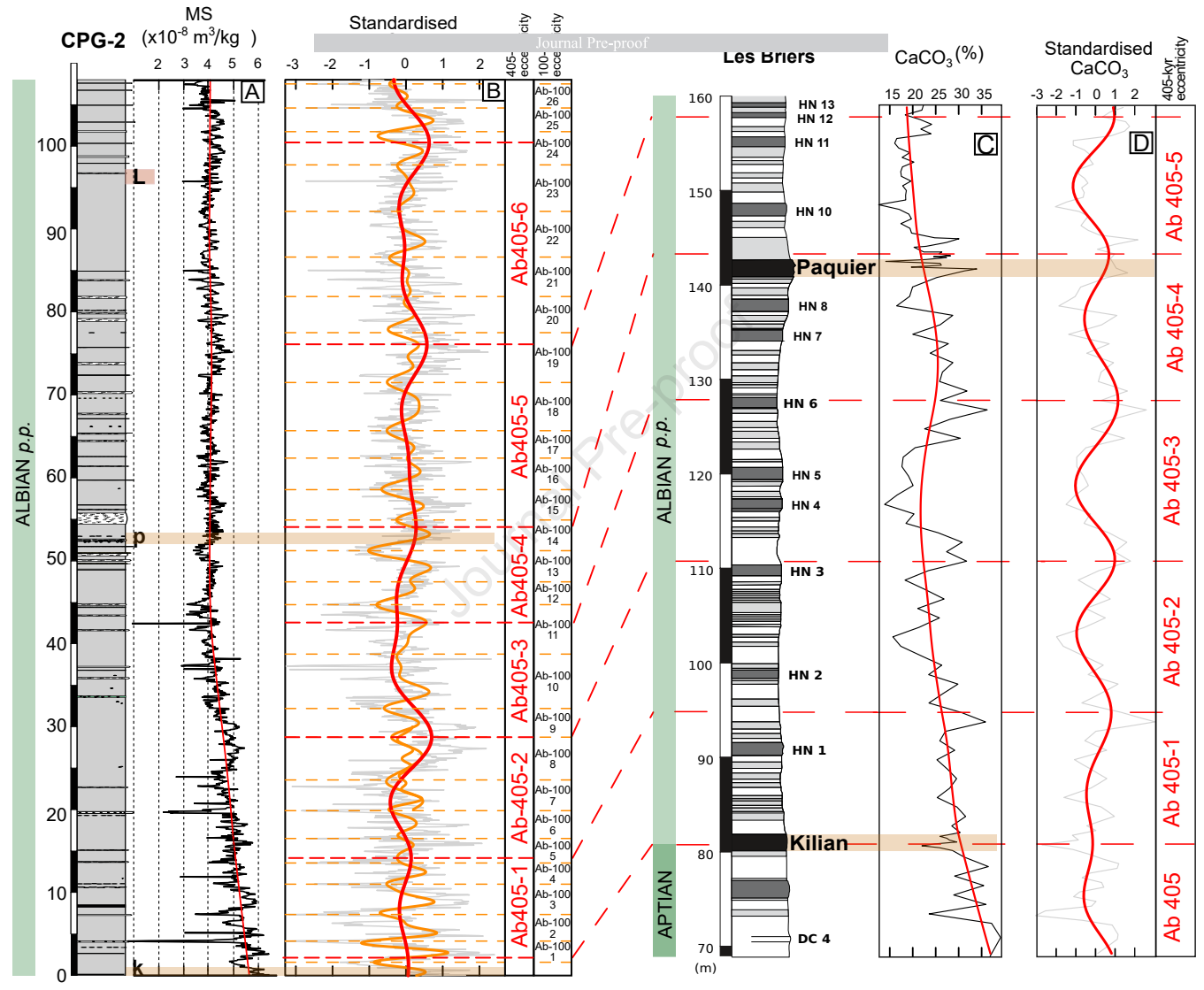
CPG-2
MS
(x10-8 m3/kg)
A
B
Standardised
405-kyr eccentricity
100-kyr eccentricity
Journal Pre-proof
ALBIAN p.p.
L
p
k
Ab405-6
Ab405-5
Ab405-4
Ab405-3
Ab-405-2
Ab405-1
Les Briers
HN 13
HN 12
HN 11
HN 10
Paquier
HN 8
HN 7
HN 6
HN 5
HN 4
HN 3
HN 2
HN 1
Kilian
DC 4
APTIAN
(m)
CaCO3 (%)
C
Standardised CaCO3
D
405-kyr eccentricity
Ab 405-5
Ab 405-4
Ab 405-3
Ab 405-2
Ab 405-1
Ab 405

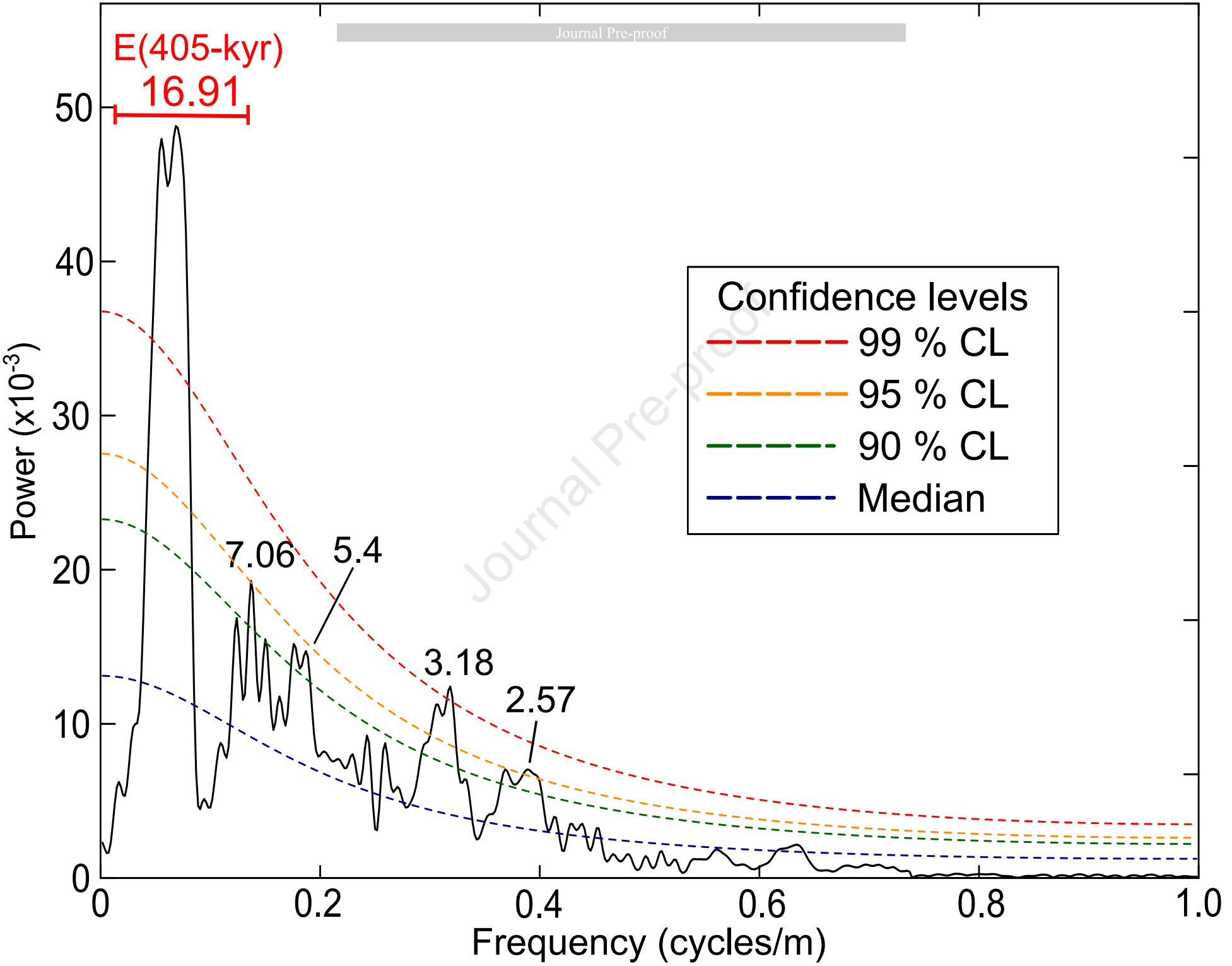
E(405-kyr)
16.91
Journal Pre-proof
Confidence levels
99 % CL
95 % CL
90 % CL
Median
7.06
5.4
3.18
2.57
Power (x10-3)
Frequency (cycles/m)
0
10
20
30
40
50
0
0.2
0.4
0.6
0.8
1.0

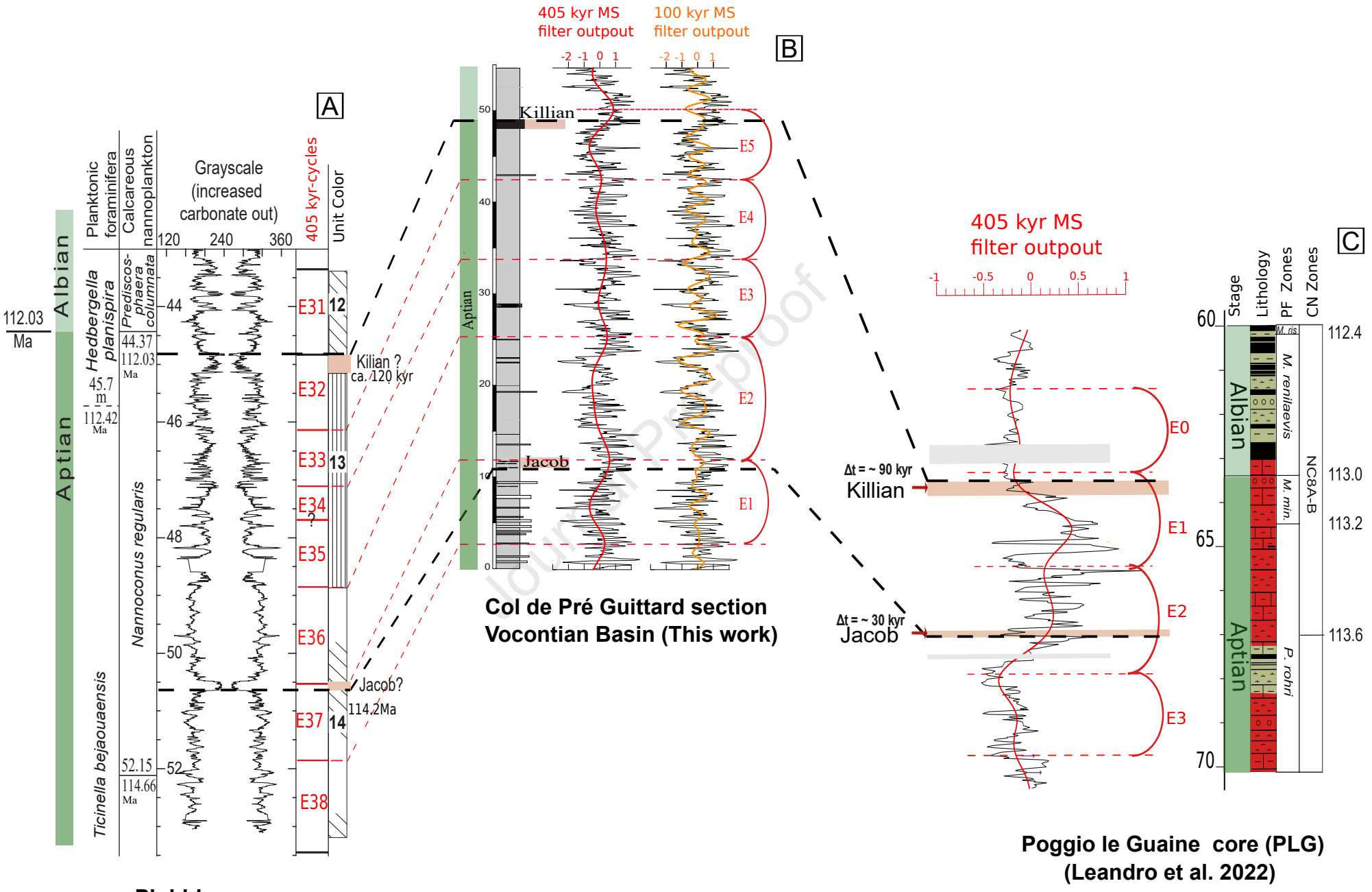

Piobbico core
Central Italy
(Huang et al. 2010)

Col de Pré Guittard section
Vocontian Basin (This work)

Poggio le Guaine core (PLG)
(Leandro et al. 2022)

Highlights

• Astronomical calibration of the OAE 1b interval in Col de Pré-Guittard section, GSSP of the Albian.

• Jacob, Kilian, Paquier and Leenhardt events located near maximums of the 405-kyr eccentricity cycle in magnetic susceptibility

• Concomitant impact of 405-kyr eccentricity and volcanism on the onset of these events

Declaration of interests

☐ The authors declare that they have no known competing financial interests or personal relationships that could have appeared to influence the work reported in this paper.

☒ The authors declare the following financial interests/personal relationships which may be considered as potential competing interests:

Ait-Itto Fatima-Zahra reports financial support was provided by Make our planet great again (MOPGA). Mathieu Martinez reports financial support was provided by National Centre for Scientific Research MITI Le Temps AstroCarb. AIT-ITTO Fatima-Zahra reports financial support was provided by project SAD METOX from Région Bretagne. Mathieu Martinez reports financial support was provided by Défis Scientifiques program from Université de Rennes.